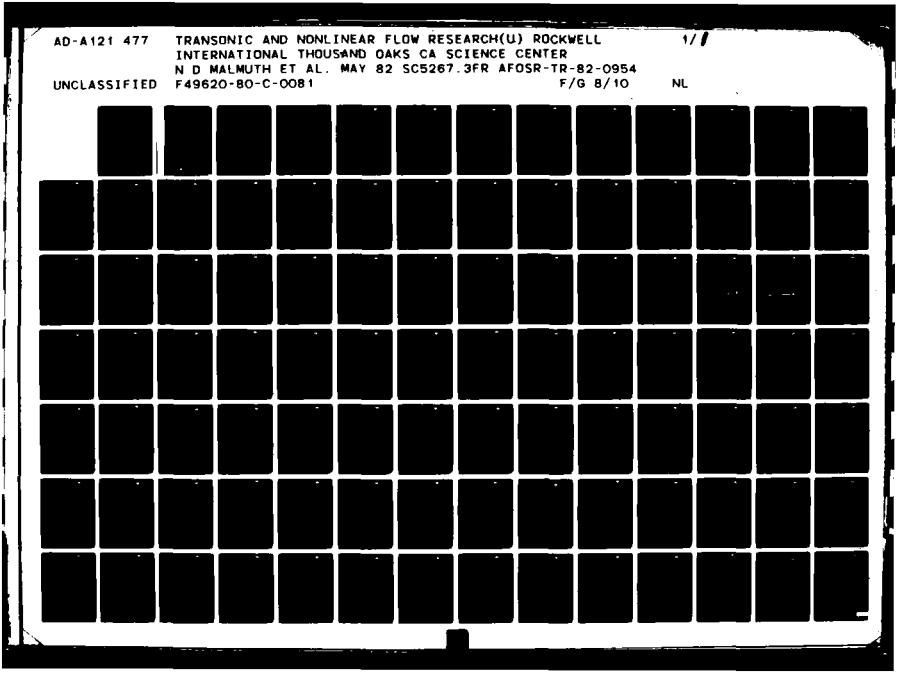
AD-A121 477 TRANSONIC AND NONLINEAR FLOW RESEARCH(U) ROCKWELL 1/1
INTERNATIONAL THOUSAND OAKS CA SCIENCE CENTER
N D MALMUTH ET AL. MAY 82 SC5267.3FR AFOSR-TR-82-0954
UNCLASSIFIED F49620-80-C-0081 F/G 8/10 NL

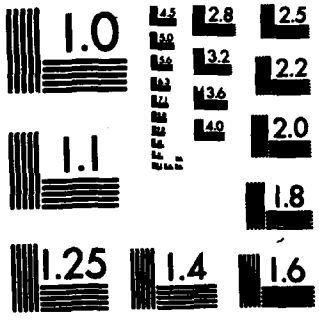

Report No. SC5267.3FR

TRANSONIC AND NONLINEAR FLOW RESEARCH

N.D. Malmuth
Rockwell International Science Center
Thousand Oaks, California 91360

J.D. Cole and C.C. Wu
University of California at Los Angeles
Los Angeles, California 90024

and

F. Zeigler
University at Wisconsin Mathematics Research Center
Madison, Wisconsin
May, 1982

Final Report for Period June 1, 1980 through February 28, 1982

Prepared for

Air Force Office of Scientific Research
Building 410
Bolling AFB, D.C. 20332

This research was sponsored by the Air Force Office of Scientific Research under Contract No. F49620-80-C-0081, Project No. 2307/A1

Rockwell International
Science Center

UNCLASSIFIED

SECURITY CLASSIFICATION OF THIS PAGE (When Data Entered)

REPORT DOCUMENTATION PAGE		READ INSTRUCTIONS BEFORE COMPLETING FORM
1. REPORT NUMBER AFOSR-TR- 82-0954	2. GOVT ACCESSION NO. AD-A112 470	3. RECIPIENT'S CATALOG NUMBER
4. TITLE (and Subtitle) TRANSONIC AND NONLINEAR FLOW RESEARCH		5. TYPE OF REPORT & PERIOD COVERED Final report for period 06/01/80 thru 02/28/82
		6. PERFORMING ORG. REPORT NUMBER SC5267.3FR
7. AUTHOR(s) N.D. Malmuth, J.D. Cole, C.C. Wu, and F. Zeigler		8. CONTRACT OR GRANT NUMBER(s) F49620-80-C-0081
9. PERFORMING ORGANIZATION NAME AND ADDRESS Rockwell International Science Center P.O. Box 1085 Thousand Oaks, California 91360		10. PROGRAM ELEMENT, PROJECT, TASK AREA & WORK UNIT NUMBERS 2307/A1 61102F
11. CONTROLLING OFFICE NAME AND ADDRESS Director of Aerospace Sciences Air Force Office of Scientific Research, Bldg. 410 Bolling AFB, D.C. 20332		12. REPORT DATE May, 1982 13. NUMBER OF PAGES 93
14. MONITORING AGENCY NAME & ADDRESS(if different from Controlling Office)		15. SECURITY CLASS. (of this report) Unclassified 15a. DECLASSIFICATION/DOWNGRADING SCHEDULE

16. DISTRIBUTION STATEMENT (of this Report)

Approved for public release; distribution unlimited.

17. DISTRIBUTION STATEMENT (of the abstract entered in Block 20, if different from Report)

18. SUPPLEMENTARY NOTES

None

19. KEY WORDS (Continue on reverse side if necessary and identify by block number)

Transonic flow, asymptotic expansions, wind tunnels, optimization, inviscid flow, computational fluid dynamics

20. ABSTRACT (Continue on reverse side if necessary and identify by block number)

The research program consists of the investigation of transonic slender body theory and optimization procedures as well as asymptotic methods for wind-tunnel interference in the supercritical regime. For the slender body portion, two areas received attention. In the first, the existence of an unsteady equivalence rule has been verified in which the outer solution is governed by axisymmetric unsteady small disturbance theory subject to an unsteady line source internal boundary condition and far field. As in the

DD FORM 1 JAN 73 1473

UNCLASSIFIED

SECURITY CLASSIFICATION OF THIS PAGE (When Data Entered)

steady case, the strength of the line source depends on an inner solution for the potential, which is harmonic in cross planes to the flow. This solution specifies the line source intensity in terms of a rate of change of the cross sectional area distribution in which the unsteady motion of the body surface is taken into account.

The second aspect of the research effort deals with optimization of slender lifting wing-body combinations. A restricted class of these shapes has been considered in which the wing span increases monotonically from a common apex with the body. For pointed tails, the aerodynamic efficiency can be maximized by minimization of the wave drag. A parameterized inverse (PI) procedure is utilized to demonstrate substantial decreases in this quantity. The PI method employs a parameterized fairing of the surface pressure distribution about a discontinuous one associated with a surface shock. The parameters are adjusted to minimize the drag and satisfy constraints such as specified thickness, and base area as well as closure as a special case. With the procedure, the question of the existence of supercritical shock-free axisymmetric bodies has been addressed. The examples investigated suggest that such shapes can be found. Other results demonstrate that surface smoothing of the pressure will not be synonomous with the wave drag elimination due to focusing and envelope formation of the wave system off the body.

For the wall interference portion of the effort, the method of matched asymptotic expansions is utilized to study the singular perturbation problem relevant to transonic airfoils confined by large height to chord ratio solid walls. In this class of flows, the (inner) near field is represented as a linear perturbation about the nonlinear free field which is assumed to be governed by the Karman-Guderley small disturbance theory which is non-uniformly valid as the walls are approached. In the far field (outer) region, another approximate representation of the wall-airfoil interaction involving a multipole, dominated by a vortex reflected between the walls is valid. Through the use of intermediate limits, matching of both representations is demonstrated. Some numerical solutions for the inner problem are illustrated in which the inner limit of the outer solution is employed as a far field boundary condition for the perturbed flow. Means of correcting the tunnel incidence to obtain an interference-free value for the lift are demonstrated from the examples. By virtue of the nature of the perturbation method, the height dependence is separated out from the problem and universal correction functions are available from the theory for airfoils at given incidence and Mach number conditions.

TABLE OF CONTENTS

TABLE OF CONTENTS (Continued)

LIST OF TABLES

Part 1

Part 2

LIST OF ILLUSTRATIONS

Part 1

LIST OF ILLUSTRATIONS (Continued)

FOREWORD

This document constitutes the final report for AFOSR Contract F49620-80-C-0081A for the period June 1, 1980 to May 1, 1982. Contained herein is a summary of research in two areas: asymptotic theory of transonic wind tunnel interference as well as slender body theory and optimization. Each of the topics employs an integrated approach consisting of asymptotic and numerical procedures useful in describing the flow. Actually, both subjects are interrelated, since the three-dimensional wind tunnel problem for many configurations embodies many of the asymptotic ideas arising in slender body theory and the equivalence rule.

This report is written in two separate sections relevant to the previously enumerated areas. These give a fairly detailed account of the research effort in each. Principal outcomes of the program are the following:

- A systematic asymptotic theory for solid wall interference over two-dimensional airfoils
- A new unsteady version of the equivalence rule
- A means of optimizing transonic lifting wing bodies in steady flow and the first solution our knowledge of the axisymmetric inverse problem with closure allowing "nonlinear area ruling"
- New results for the nonlinear component of the far field around lifting airfoils at transonic speeds.

The work on transonic wind tunnel wall interference is a natural outcome of activity on tunnel wall far fields under previous contracts.

In addition to the description of accomplishments, suggestions for future effort are provided.

PART 1

SLENDER BODY THEORY AND OPTIMIZATION PROCEDURES AT TRANSONIC SPEEDS*

SUMMARY

Two areas have been investigated within transonic slender body theory. In the first, the existence of an unsteady equivalence rule has been verified in which the outer solution is governed by axisymmetric unsteady small disturbance theory subject to an unsteady line source internal boundary condition and far field. As in the steady case, the strength of the line source depends on an inner solution for the potential, which is harmonic in cross planes to the flow. This solution specifies the line source intensity in terms of a rate of change of the cross sectional area distribution in which the unsteady motion of the body surface is taken into account.

The second portion of the research effort deals with optimization of slender lifting wing-body combinations. A restricted class of these shapes has been considered in which the wing span increases monotonically from a common apex with the body. For pointed tails, the aerodynamic efficiency can be maximized by minimization of the wave drag. A parameterized inverse (PI) procedure is utilized to demonstrate substantial decreases in this quantity. The PI method employs a parameterized fairing of the surface pressure distribution about a discontinuous one associated with a surface shock. The parameters are adjusted to minimize the drag and satisfy constraints such as specified thickness, and base area as well as closure as a special case. With the procedure, the question of the existence of supercritical shock-free axisymmetric bodies has been addressed. The examples investigated suggest that such shapes can be found. Other results demonstrate that surface smoothing of the pressure is synonomous with wave drag elimination due to focusing and envelope formation of the wave system off the body.

*Material from this section will be submitted to the AIAA Journal for publication in the future.

1.0 INTRODUCTION

During the 1950's, techniques were developed to analyze and design aircraft to accelerate through what was then called the sound barrier. The procedure employed was an "area rule"[1] in which the drag of a complete airplane was computed from that of an equivalent body of revolution. A related development with the Oswatitsch equivalence rule[2] which was later further enunciated by Spreiter and Heaslet in Ref. 3. Therein, cases were considered in which the incidence was small with respect to the thickness. This approximation leads to a well known further decomposition for transonic flows which is indicated schematically in Fig. 1. As shown, the nonlinear embodiment involves the solution of two problems. The first is the nonlinear flow over an equivalent body of revolution and the second, a cross flow problem which can in turn be decomposed into a steady asymmetric cross flow and an unsteady symmetric flow associated with the cross section expanding at the rate at which the flow moves downstream.

In spite of its well developed status, the Jones-Whitcomb area rule in which the equivalent body of revolution problem is linear, rather than nonlinear, can lead to suboptimal design solutions. Despite the relative weakness of shocks occurring in mixed flows, small drag changes carry important mission implications. An accurate means of drag estimation as well as a systematic optimization procedure is required, particularly, when the assumptions of Prandtl-Glauert theory are violated.

As one method of handling nonlinear effects, constrained minimization has provided a useful means of optimizing transonic shapes under certain circumstances. In this procedure, the body shape is expressed in terms of a finite number of parameters. The nonlinear problem for the optimization of some aerodynamic quantity such as drag or aerodynamic efficience as a functional of these parameters is solved in which an extremum is sought in the space of these variables using decision theory. Unfortunately, the computational effort required to obtain such a solution is great, and only a local rather than global optimum is usually obtained in this manner.

SC82-16838

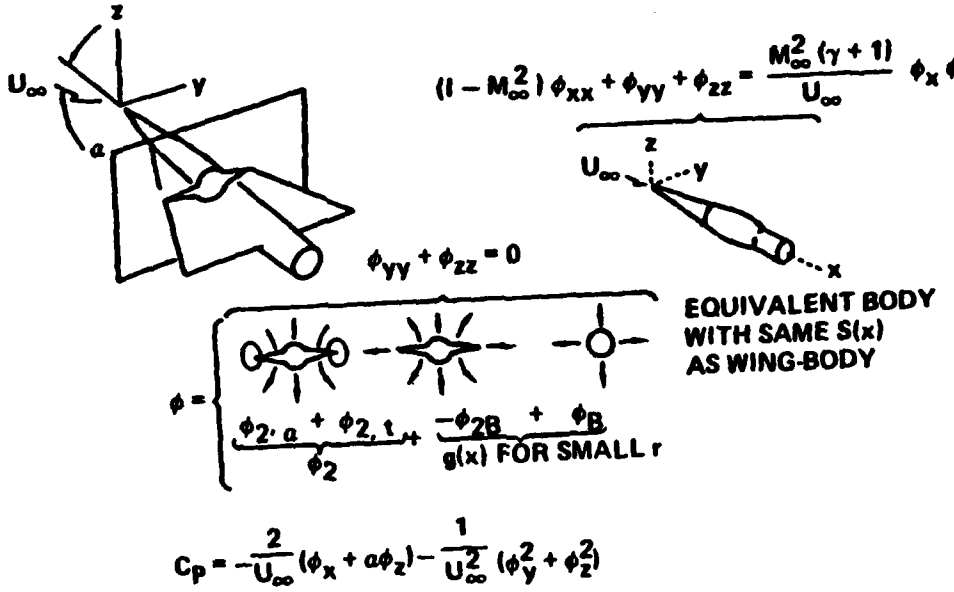

Fig. 1. Transonic equivalence rule

Because of these deficiencies, a need exists for other methods. One group of interest deals directly with desirable loading features during the optimization process. A typical example occurs in transonic airfoil theory in which nearly shockless surface pressure distributions and minimization of adverse pressure gradients are obtained by a technique known as the inverse method. At the Science Center, the approach has reached a high degree of refinement for airfoil and wing problems. An account of its current status is given in Ref. 4. Application to laminarization is discussed therein as well as the aspect of closure.

In the design or inverse procedure, shapes are sought supporting preassigned pressure distributions in contrast to the direct or analysis method where the reverse is true. A typical implementation is to smooth out jump discontinuities in the surface pressure distribution that would be associated with shocks. In principle, this process could lead to a reduction in wave drag. However, it is not obvious that the elimination of such a surface discontinuity will be synonomous with removal of the shocks off the body. In this respect, constrained minimization has an advantage, since it deals directly with a concomitant of the shock, the wave drag. We believe that further understanding of the envelope formation process leading to this discontinuity, in concert with the inverse method, could overcome this deficiency and provide it with even greater power to solve the optimization problem.

On the basis of the equivalence rule and the inverse capability, an attractive possibility occurs regarding optimization of slender airplanes. This notion has stimulated the application of the technology to the equivalent body of revolution component indicated in Fig. 1 in the research effort to be described. Since the wave drag arises solely from this contribution, a potent means of improving aerodynamic performance is available with simplified versions of modern computational methods. Here, the reduction in complexity arises from the dominant axial symmetry of the asymmetric slender problem in the nonlinear part of the flow.

In what follows, an account of the research concerning the solution of the inverse problem for slender configurations is given. Prior to this discussion, a description of an unsteady equivalence rule will also be provided. Herein, the basic methods developed in Ref. 5 are generalized to an unsteady context. Future applications for the modeling of flows relevant to aerodynamic applications are indicated in this connection. For the steady portion of the activities, the application of the optimization procedures to achieve minimum wave drag are described as well as salient issues dealing with constraints. In addition, the implication of wave drag reduction measures relative to aerodynamic efficiency is also given pointing to the need for further efforts which are also indicated.

2.0 ANALYSES

2.1 Unsteady Equivalence Rule

Basic Equations

Denoting $\vec{q}$ the vector velocity ρ the density, P, the pressure, T the time and $\frac{D}{DT}$ the substantial derivative, the continuity and momentum equations for inviscid flow are respectively

$$\nabla \cdot \rho \vec{q} = 0 \tag{1a}$$

$$\frac{D\vec{q}}{DT} = -\frac{\nabla P}{\rho} = \vec{q}_T + \frac{\nabla q^2}{2} \quad , \tag{1b}$$

where subscripts denote differentiation, $q^2 \equiv |q|^2$ and irrotationality has been assumed. If the flow is considered to be constant state and adiabatic in the freestream, the energy invariant in isentropic flow is

$$\Phi_T + \frac{q^2}{2} + \frac{a^2}{\gamma-1} = f(T) = \frac{U^2}{2} + \frac{a_\infty^2}{\gamma-1} = C^2 \quad , \tag{1c}$$

where Φ is the velocity potential, U is the freestream speed, a is the speed of sound, subscript ∞ denotes a freestream quantity, and C and f are independent of T because of the freestream conditions assumed. Substituting (1c) into (1b) gives

$$a^2 \nabla \cdot \vec{q} - \vec{q} \cdot \nabla \left\{ \Phi_T + \frac{q^2}{2} \right\} = \Phi_{TT} + \left(\frac{q^2}{2} \right)_T \tag{1c'}$$

where

$$q^2 = \Phi_X^2 + \Phi_R^2 + \frac{1}{R^2} \Phi_\theta^2 \quad ,$$

for cylindrical coordinates, in which R,θ are polar coordinates

in planes perpendicular to the X axis which is aligned with the free-stream. From (1c') the full potential equation is then

$$\left(a^2-\Phi_X^2\right)\Phi_{XX} + \left(a^2-\Phi_R^2\right)\Phi_{RR} + \frac{a^2\Phi_R}{R} + \left(a^2-\frac{\Phi_\theta^2}{R^2}\right)\frac{\Phi_{\theta\theta}}{R^2} - 2\Phi_X\Phi_R\Phi_{RX}$$

$$- \frac{2\Phi_X\Phi_\theta\Phi_{\theta X}}{R^2} - \frac{2\Phi_\theta\Phi_R\Phi_{\theta R}}{R^2} - 2\Phi_R\Phi_{TR} - 2\Phi_X\Phi_{TX} - \frac{2}{R^2}\Phi_\theta\Phi_{T\theta}$$

$$- \frac{2\Phi_\theta^2\Phi_R}{R^3} - \Phi_{TT} = 0 \quad . \tag{2}$$

Transonic Unsteady Small Disturbance Theory

Heuristically asserting that the asymptotic structure is similar to that of steady flow, an outer expansion representing the flow at moderate distances from the slender body can be written as

$$\Phi = U\left\{X+c\delta^2\phi(x,\tilde{r},\theta,\tilde{t}) + \ldots \right\} \tag{3a}$$

where c is the body length, δ is the body thickness ratio, and

$$x = \frac{X}{c}, \quad \tilde{r} = \frac{\delta R}{c}, \quad \tilde{t} = \delta^2\frac{UT}{c}, \quad K = \frac{1-M_\infty^2}{\delta^2} \text{ fixed as } \delta \to 0 \quad , \tag{3b}$$

in the outer limit for validity for (3a). On substitution of (3a) into (2), the unsteady small disturbance equation

$$[K-(\gamma+1)\phi_x]\phi_{xx} + \frac{1}{\tilde{r}}(\tilde{r}\phi_{\tilde{r}})_{\tilde{r}} + \frac{\phi_{\theta\theta}}{\tilde{r}^2} - 2\phi_{x\tilde{t}} = 0 \tag{4}$$

is obtained. As in the steady case, the preliminary assertion is made (pending matching) that the $\tilde{r}$ derivative term dominates (4) as $\tilde{r} \to 0$. This leads to the condition

$$\lim_{\tilde{r} \to 0} \tilde{r}\phi_{\tilde{r}} = S(x,\tilde{t},N,\Omega) \qquad (5)$$

where N and Ω are dimensionless amplitude and frequency parameters. These quantities arise naturally in the boundary conditions to be described. Besides (5), additional conditions necessary to determine the solution of (4) involve the wake and far field. Since our focus is primarily the existence of an unsteady equivalence rule, the latter will be only briefly and qualitatively indicated here. For a subsonic far field, it is reasonable to assume that an unsteady version of the line source expression given in Ref. 7 will be applicable. The condition on the wake is determined from an inner expansion in a region close to x axis. The need for this representation is associated with a non-uniformity of the outer expansion associated with a logarithmic behavior given by an integral form of (5), i.e.,

$$\phi \simeq S(x,\tilde{t})\ell n\tilde{r} + g(x,\tilde{t}) \quad \text{as } r^2 \to 0. \qquad (5')$$

Formalizing this idea and following Ref. 5, the appropriate representation is

$$\Phi = U\left\{X + \delta^2 c\phi^*(x,r^*,\theta,\tilde{t},K,\Omega,N) + \ldots\right\} \quad , \qquad (6a)$$

which is assumed valid in an inner limit

$$x,r^* = r/\delta \ , \ \tilde{t} = \delta^2 t \quad \text{fixed as } \delta \to 0 \quad . \qquad (6b)$$

On substitution of (6b) in (2), the steady cross flow Laplacian equation is obtained as in the steady case as

$$\phi^*_{r^*r^*} + \frac{\phi^*_{r^*}}{r^*} + \frac{1}{r^{*2}}\phi^*_{\theta\theta} = 0 \quad , \qquad (7)$$

where the (r^*,θ) polar coordinate system in a typical cross flow plane is shown in Figs. 2 and 3a. If $B(x,\tilde{r},\tilde{t}) = 0$, denotes the body surface, the tangency conditions for (7) is

$$B_{\tilde{T}} + \vec{q} \cdot \nabla B = 0 \quad . \tag{8}$$

If, furthermore, B is written in the form

$$B = R - \delta c F(x,\theta,T) = 0 \quad , \tag{9}$$

and noting that

$$\frac{\vec{q}}{U} = (1+\delta^2\phi^*_x + \ldots)\,\vec{i}_x + \delta\phi^*_{r^*}\vec{i}_{r^*} + \frac{\delta\phi^*_\theta}{r^*}\,\vec{i}_\theta + \ldots \quad , \tag{10}$$

where $\vec{i}_x, \vec{i}_r$ and $\vec{i}_\theta$ are unit vectors in the indicated directions, substitution of (9) and (10) into (8) yields on retention of terms to $O(\delta)$ the relation

$$\left(\phi_{r^*} - \frac{F_\theta}{F}\,\phi^*_\theta\right)\Big|_{r^*=F} = F_x(x,\theta,\tilde{t}) + \delta^2 F_{\tilde{t}}(x,\theta,\tilde{t}) \simeq F_x(x,\theta,\tilde{t}) \quad , \tag{11}$$

$$\left(t \equiv \frac{UT}{c}\right)$$

where $r^* = F$ is the body cross sectional boundary in the cross flow plane shown in Fig. 3. In typical cases, the function F can be written as

$$F = f(x,\theta,a\sin\Omega\tilde{t}) = f(x,\theta,a\sin\omega t) \tag{12}$$

$$\Omega = \frac{\omega}{\delta^2} = O(1) \text{ as } \delta \to 0 \quad .$$

where if $\bar{\omega}$ is the dimensional frequency, $\omega = \frac{\bar{\omega}c}{U}$, and a is an amplitude in units of δc. Some examples follow:

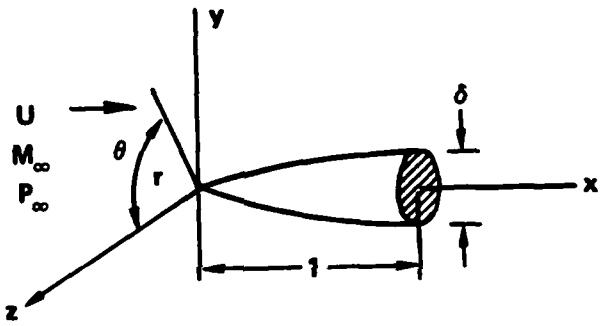

Fig. 2. Slender body geometry

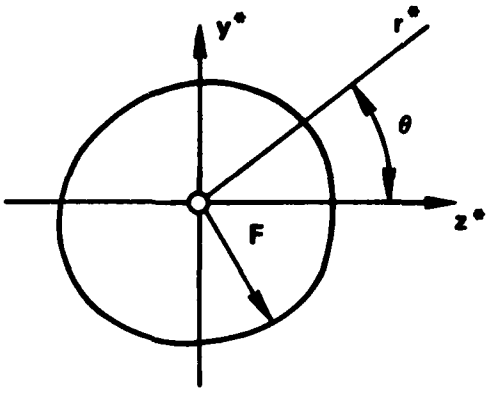

Fig. 3a. Body cross section geometry

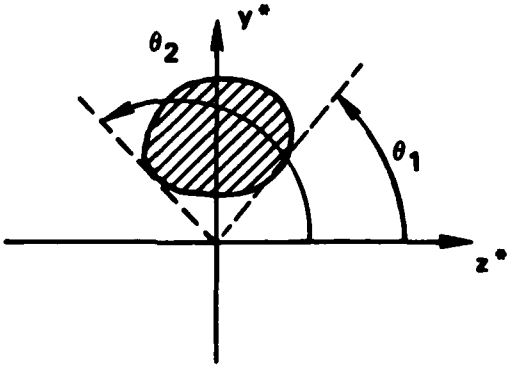

Fig. 3b. Non star-shaped region in cross flow plane

Harmonic Dilatation

$$f = a\sin\omega t\, G(x,\theta) \tag{13a}$$

where aG is cross sectional shape at $\omega t = \frac{\pi}{2}$

Harmonic Pitch and Plunge

$$f = ax^n \sin\omega t \sin\theta + \sqrt{G^2(x,\theta) - a^2x^{2n}\sin^2\omega t\cos^2\theta} \tag{13b}$$

where G is the cross sectional shape in the pitching or plunging frame, n = 0 for plunge and n = 1 for pitch, and imaginary values of the radical in (13b) apply to θ values outside of the range $\theta_1 \leq \theta \leq \theta_2$ shown in Fig. 3b. Specialization of (8) to (13b) indicates that the quantity a must be $O(1)$ in order that both terms of the left hand side of (11) are also $O(1)$.

For motions given by (12) and in particular, these examples,

$$F_x + \delta^2 F_{\tilde{t}} = F_x + NF_{(3)}\cos\Omega\tilde{t} \quad , \tag{14}$$
$$\approx F_x$$

where $\frac{\partial}{\partial(3)}$ represents differentiation with respect to the third argument, and $N = a\Omega\delta^2 = O(\delta^2)$ since a, Ω have been assumed to be $O(1)$. If $\Omega = O(1)$ and $a = O(\delta^{-2})$, unphysically large amplitudes would occur, or the radial variation would dominate the circumferential ones in the left side of (11), departing from desired generality. If $\Omega = O(\delta^{-2})$, with $a = O(1)$, then additional temporal derivative terms would be required in the equations of motion and the boundary conditions as in the linear case. Note that for planar flows, (of Eq. (4-7) of Ref. 6), the expression analogous to (14) *does* contain the second term involving an amplitude parameter such a N. There, the inclusion does not lead to large amplitudes.

Using identical procedures to that given in Ref. 5, the boundary condition (14) can be written as the following Neumann condition in the cross plane:

$$\left.\frac{\partial\phi^*}{\partial n}\right|_{r^*=F} = \frac{FF_x}{\sqrt{F_\theta^2+F^2}}$$

This is explicitly the same boundary condition (except with $\tilde{t}$ dependencies) as for the steady-state inner solution of Ref. 5. Using Green's theorem as in Ref. 5, the asymptotic behavior of ϕ^* for large r^* is

$$\phi^* = \frac{1}{2\pi} (\ell n r^*) A_x \quad , \tag{16a}$$

where

$$A = \frac{1}{2} \int_0^{2\pi} F^2 d\theta \quad . \tag{16b}*$$

In accord with the previous remarks, the complete inner solution can be written as

$$\phi^* = S^*(x,\tilde{t}) \log r^* + g^*(x,\tilde{t}) + \sum_{n=1}^{\infty} \frac{g_n(x,\tilde{t})\cos n\theta + f_n(x,\tilde{t})\sin n\theta}{r^{*n}} \quad . \tag{17}$$

The matching procedures developed in Ref. 5 applied here give the following results

$$S(x,\tilde{t}) = S^*(x,\tilde{t}) = \frac{1}{2\pi} A_x \tag{18a}$$

*The limits shown are applicable if $r^*=F$ encloses the origin as a star shaped region, i.e., $r^*=F(\theta,x)$ is a single valued function of θ. If not, then $A = \oint F^2 d\theta$, where the θ limits are selected so that the contour $r^*=F$ is traversed in the counterclockwise sense.

$$g(x,\tilde{t}) = g^*(x,\tilde{t}) \quad , \tag{18b}$$

with the inner and outer expansions given respectively by

$$\Phi_{INNER} = U\left\{X+c\left[(\delta^2 \ell og\ \delta)2S(x,\tilde{t})+\delta^2\phi(x,r^*,\tilde{t};K,\Omega) + \ldots\right]\right\} \tag{19a}$$

for (6b) and,

$$\Phi_{OUTER} = U\left\{X+c\delta^2\phi(x,\tilde{r},\tilde{t};K,\Omega) + \ldots\right\} \tag{19b}$$

for (3b), and the $\delta^2 \ell og\ \delta$ switchback term inserted for matching purposes.

From the energy invariant and isentropy, the surface pressures on the body $r^*=F$ are given by

$$-\frac{C_P}{\delta^2} = 2S_x(x,\tilde{t})\ \ell og\delta^2 F + 2g_x(x,\tilde{t}) + v_B^2 + w_B^2 \tag{21a}$$

where

$$v_B = \frac{S}{F} - \sum_{n=1}^{\infty}\frac{g_n cosn\theta + f_n sinn\theta}{F^{(n+1)}} \tag{21b}$$

$$w_B = \sum_{n=1}^{\infty}\frac{n\left\{-g_n sinn\theta + f_n cosn\theta\right\}}{F^n} \tag{21c}$$

in which g_n and f_n are functions of x and $\tilde{t}$.

Summary - Unsteady Equivalence Rule

The unsteady equivalence rule is embodied in Eqs. (21) in which

$$g = \lim_{\tilde{r} \to 0} \left\{ \phi(x,\tilde{r},\tilde{t}) - S(x,\tilde{t}) \log \tilde{r} \right\} \tag{22}$$

with S determined by (18a) and ϕ the outer perturbation potential is the solution of the unsteady small disturbance equation (4), in which $\frac{\partial}{\partial \theta} = 0$, due to the equivalent body of *revolution boundary condition* (5). The wake condition by symmetry is

$$\phi_{\tilde{r}}(x,0,\tilde{t}) = 0 \quad , \quad x > 1 \tag{23}$$

in the solution of the outer problem.

In a practical application, the procedure described previously could be utilized to compute transonic unsteady flows over low aspect ratio configurations such as fighter arrangements. To obtain a truly useful tool however, generalizations are required to handle shapes in which the wings are non-monotonically increasing in span from the nose of the wing-body arrangement. For these cases, the wakes play an important role, modifying the autonomy of downstream sections. As in steady interactions, the higher order matching is important, including a theory of the materialization of shocks in the near field.

2.2 Steady Slender Body Theory and Optimization Studies

The previous results when specialized to steady flow can be used to study L/D optimization of wing-body configurations of the type shown in Fig. 4. Here, the body has a circular cross section, and the wing is increasing monotonically from the pointed apex to the base section and is of zero thickness. Based on Ref. 5 and 8, the aerodynamic efficiency at an angle of attack α is given as

$$\frac{L}{D} = \frac{2\pi(s^2 - R_0^2 + R_0^2/s^2)\alpha}{\delta^* \{B+I\}} \tag{24a}$$

where

$$B = \pi S(1)g(1) - \frac{1}{2}\int_0^{2\pi} \phi^*(1,F,\theta)FF_x(1,\theta)d\theta - \left[\log \delta\right]\left[2\pi S^2(1)\right] \tag{24b}$$

$$I = -2\pi\int_0^1 S(x)g'(x)dx \tag{24c}$$

R_0 = body base radius in units of the chord

s = span at base in units of the chord,

and g and S are steady specializations of that given in (22) and (18a). In general, the specification of a fixed base could be driven by an engine packaging requirement or RCS considerations.

SC82-16843

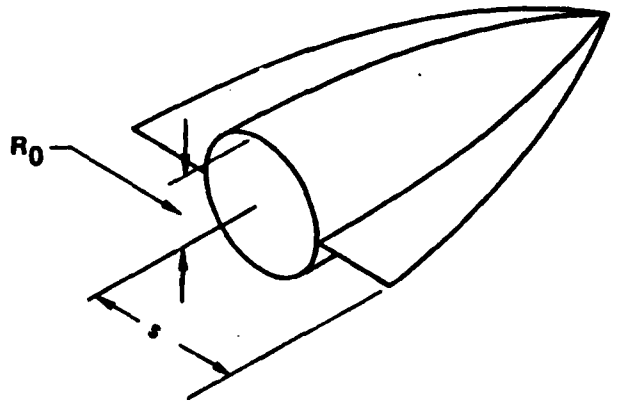

Fig. 4. Basic configuration for L/D optimization studies

In the research conducted during the course of the program a major emphasis was placed on drag reduction associated with the minimization of the denominator in (24a). For a fixed R_0/s, (24a) indicates that the maximum L/D corresponds to a minimum wave drag. The minimization involves global dependencies that modify B through g(1) and $\phi^*(1,F,\theta)$ in (24b). To simplify the considerations, a part of the investigation was limited to a simpler situation in which $R_0=0$, i.e., the body is pointed at its tail. For this case, (24a) specializes to

$$\frac{L}{D} = \frac{s^2\alpha}{\delta^4 \int_0^1 S(x)g'(x)dx} \qquad (24a')$$

i.e., the lift is given by a wing alone value and the boundary terms are absent from the drag. For a fixed span at the base, the aerodynamic efficiency is again maximum when the denominator is minimized. For (24a'), the complicated global dependencies in the boundary terms are not present.

To meet the foregoing minimization requirement, an effort in developing and applying special methods to derive pointed bodies supporting shockless surface pressure distributions will be described. These procedures are different than another one that evolved in an early phase of this effort and was reported in Ref. 9. The latter had the focus of dealing with certain coupling in the boundary conditions peculiar to the present axisymmetric generalization of the two-dimensional airfoil problem described in Ref. 4. In what follows, a description will be given of a new method that provides a treatment of constraints that are vital for the L/D optimization problem related to equations such as (24a) and (24a'), and in addition gives the first method of obtaining closure to our knowledge for the axisymmetric inverse problem.

This "parametrized inverse" (PI) procedure consists of the following steps:

1. Starting with a known body, the analysis boundary value problem consisting of Eqs. (4), (5), (18a) and (23) is solved to obtain a surface pressure C_p given by (21).

2. In general, the pressure distribution of Step 1 will have a discontinuity associated with a shock terminating the supersonic zone. A fourth order polynomial is used to "refair" the region in the vicinity in the shock as schematically indicated in Fig. 5. In the notation of the figure, control points at x_1 and x_2 are shown, and continuity of slope and value of C_p is required at these locations. Two parameters are introduced toward minimizing the drag C_D and obtaining closure in the sense that $F(1)=0$. (A more general case in which $F(1)\equiv F_1$ is prescribed is also discussed in what follows.) The first parameter a is the midpoint value of C_p shown in Fig. 5, i.e., $C_p(x_3)$. The second, is the intensity μ of the leading edge singularity, where for bodies pointed at the nose and tail, according to (21a),

$$C_{p_b} \ (\text{if } F \sim 1\pm x) = \mu \ell og(1\pm x) \text{ as } x \to \mp 1, \tag{25}$$

and the subscript b refers to the body value. A C_p variation near the nose of a symmetric parabolic arc body illustrating this behavior is shown in Fig. 6, where the freestream Mach number $M_\infty = 0.98$ and the thickness ratio $\delta = 0.167$. It can be seen that the numerical procedure tracks the singularity quite well, except the first mesh point, which is understandable. In fact the proper strength μ is also obtained on inspection of the slope of the curves and (5').

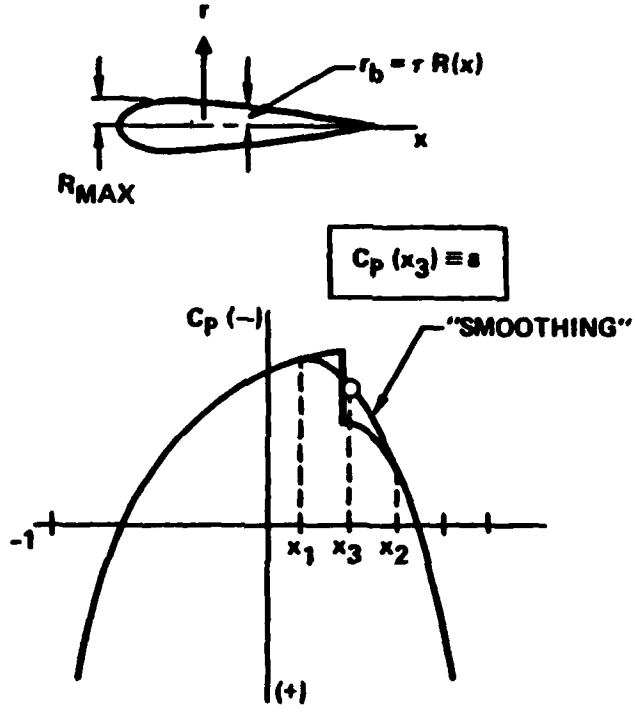

Fig. 5. Fourth order smoothing used for refairing shocked surface pressure distributions

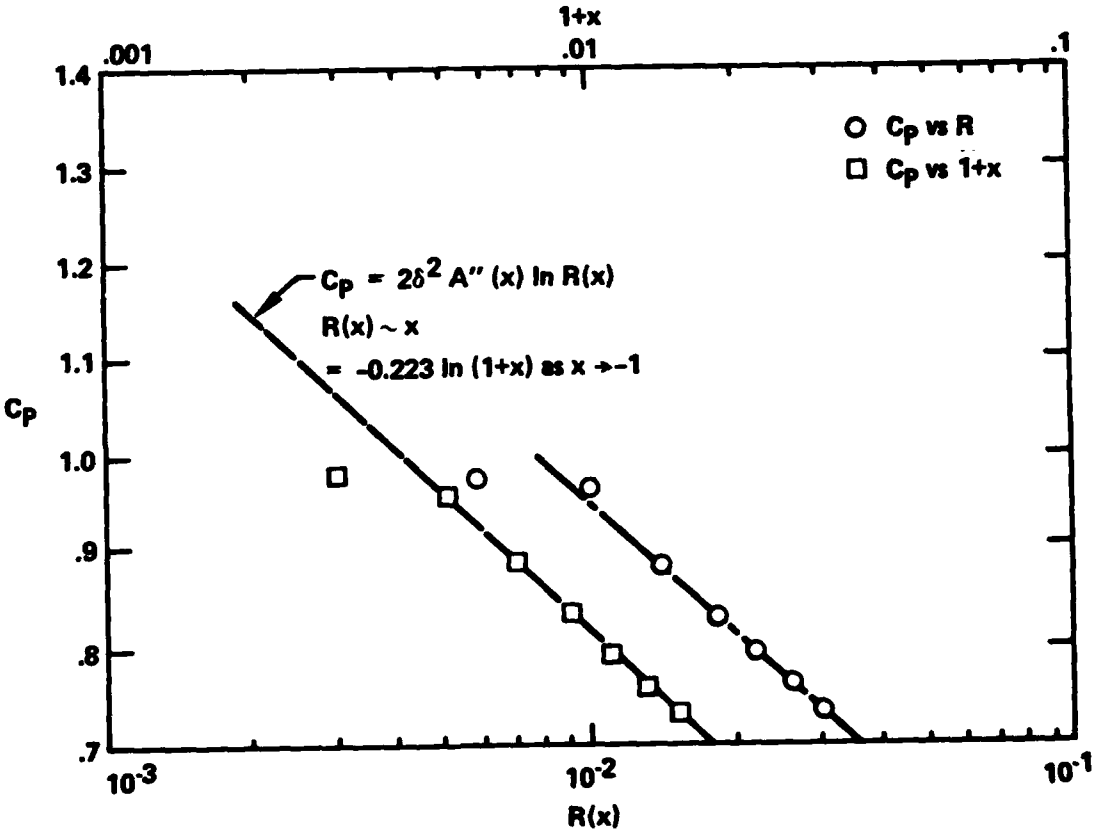

Fig. 6. Singular behavior at the nose of a fore and aft symmetric parabolic body $M_\infty = 0.98$, $\delta = 0.167$ (from SLOR solution)

3. In the iteration procedure, a given value of the parameter a is assumed as well as μ. The latter is regarded as a constant multiplicative factor for the entire $C_{P_b}(x,a,\mu)$ distribution on the interval $-1 \leq x \leq 1$.

   Regarding (21a) as an ordinary differential equation for F in which g_x is assumed known from a previous iteration, with C_P specified, $w_B=0$, and $v_B=F'$, a two point boundary value problem is solved for this equation in which

$$F(0) = F(1) = 0 \tag{26}$$

   are the boundary conditions. With g_x fixed at this stage, the solution technique is the method of bisection coupled with a Runge-Kutta integration procedure. In the implementation, two initial values of μ, μ_1, and μ_2 are obtained to bound a range where R(1) changes sign. Values of μ are changed in the left hand side of (21a) using relaxation. A set of loops are initiated in which

$$C_{P_{RELAXED}} = \Gamma C_{P_{OLD}} + (1-\Gamma)\, C_{P_{TARGET}} \tag{27a}$$

   and

$$C_{P_{NEWER}} = \mu\, C_{P_{NEW}}. \tag{27b}$$

   The ordinary differential equation (21a) is solved with (27b) and the bisection method until

$$|F(1)| < .001. \tag{27c}$$

Our experience has been that convergence is very rapid with this approach. Typical values for the μ_1 are: $\mu_1 = 0.2$ and $\mu_2 = 1.8$.

4. Once a new F distribution is obtained, the analysis algorithm described in Step 1 is used to recalculate C_p and $g'(x)$. In this step, F is relaxed in accord with the relationship,

$$\Gamma_{RELAXED} = \frac{F_{OLD} + F_{NEW}}{2} \tag{28}$$

5. Steps 3-5 are repeated until

$$C_{P_{NEW}} = C_{P_{TARGET}}.$$

6. The value of the drag coefficient is correlated against other values of the parameter a introduced in Step 3. In (27a), the value of Γ is adjusted in accord with the rule

$$\Gamma = 1 - \frac{n^2}{8+n^2} \quad , \tag{29}$$

where, $1<n<40$, and n = number of iterations. Thus, according (29), $\Gamma \to 0$ as $n \to \infty$.

7. In a recent development, the value of F is renormalized by introducing a new F in accord with the relation

$$F = \frac{F}{F_{MAX}} \tag{30}$$

Step (7) is integrated into the iteration procedure as a means of introducing a fair basis of comparison of the drag levels.

It should be noted that in the SLOR analysis code employed in Step 4, it was adequate to use only 15 sweeps before the next phase of the iteration process was initiated.

3.0 RESULTS

In what follows, illustrations of the PI method previously described to obtain shockless pressure distributions and closed axisymmetric bodies will be provided. The implications of these measures with respect to wave drag will also be addressed. Also to be indicated are calculations from algorithms devised for the satisfaction of other constraints besides closure. Viscous effects and base drag on finite base afterbodies have not been addressed here but deserve consideration in future effort. Also, basic issues of existence and uniqueness deserve attention. Another aspect investigated was the attainability of a zero wave drag body of revolution.

To show the capability of the inverse method to eliminate surface shocks, modifications of symmetric parabolic arc bodies were considered initially. Fig. 7 depicts a vertically expanded version of such a body (dashed curve) where the notation of R is used in the figures for F. The associated pressure (dashed curve) indicates a jump discontinuity produced by a shock at a location downstream of the midpoint of the body. For these calculations, 89 points were used in the x direction with 55 points across the body. In the r direction, 31 points were employed. Clustering was used in the vicinity of the nose and tail of the body for the x grid and the usual expansion of the r grid at large distances from the axis of symmetry was also applied. A smoothed pressure distribution shown as the solid curve arises from the 4th order polynomial discussed previously, where the hump is indicative of the solution for the parameter a required to achieve closure. The closure of the redesigned body shown as the solid curve is typical of the success we have had with the PI procedure in meeting this goal.

In Fig. 8, a schematic of the formation of a shock over an airfoil is shown in which the discontinuity is created by reflected waves of second family characteristics from the sonic line.

Fig. 9 indicates a typical wave system over a body of revolution. In connection with these figures, it is of interest to establish under what conditions envelopes form, and more importantly, when removal of the surface pressure discontinuity results in zero wave drag. It should be noted in this connection, that solutions of Ref. 9 as well as the PI method of this report produce reduced, but finite wave drag with smoothed surface pressure distributions. In Ref. 9, the issue of closure was not addressed. Subcritical

SC82-16844

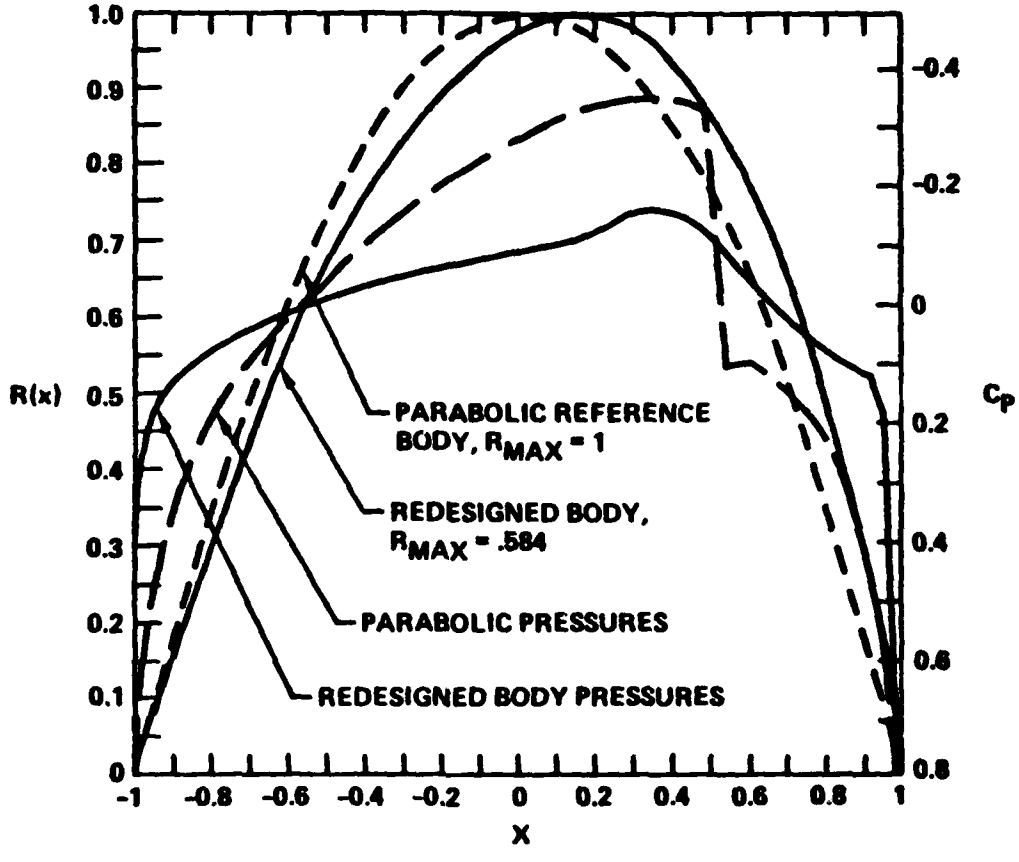

Fig. 7. Body redesign: $M = 0.98$, $\delta = 0.167$
$K = (1-M_\infty^2)/M_\infty^2\delta^2 = 1.48$, (Run 40N)

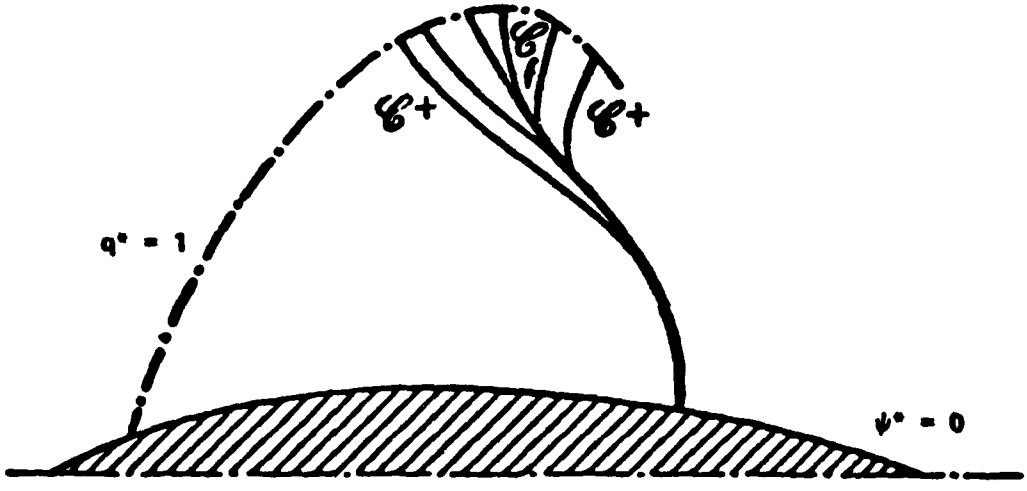

Fig. 8. Envelope formation of a shock over an airfoil

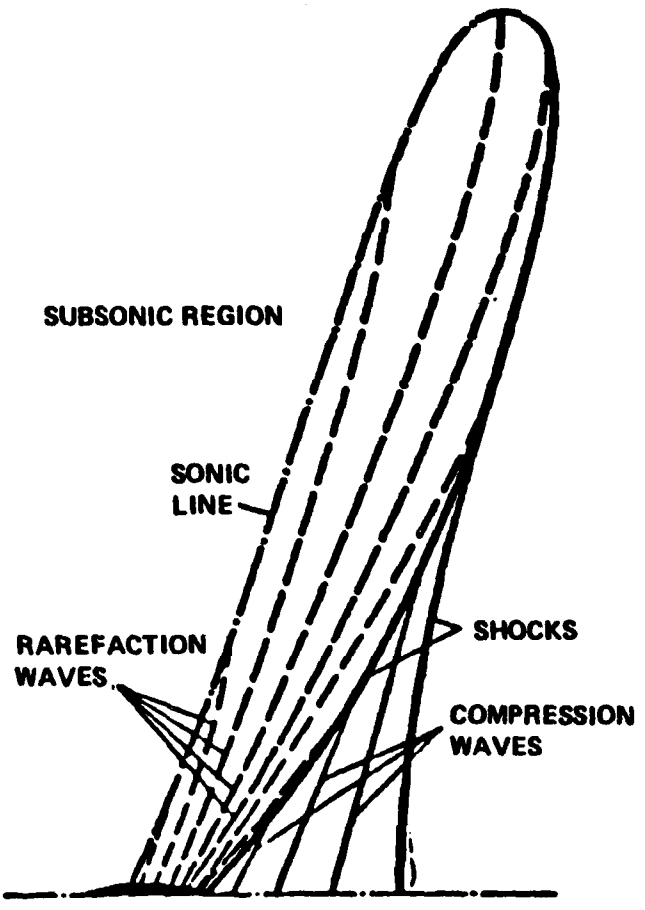

Fig. 9. Shock structure over a body of revolution

cases discussed therein demonstrated a finite drag for unclosed bodies. Since a finite base body violates the assumptions in the proof of D'Alembert's paradox, this result should not be surprising. Because the bodies can be closed in the PI method, the wave drag can be traced directly to the shock system.

Regarding the issue of drag, the basic drag coefficient C_D of the parabolic body for the case of Fig. 7 was computed to be .0459. For the refaired pressure distribution obtained in the iterations of the PI method, convergence to a value of a=-0.275 lead to C_D = 0.00022, practically zero to within the truncation error of the calculations. This result is tempered by the reduction of R_{MAX} from unity for the parabolic case, to a value of 0.524 in the refaired case. Since there is a natural reduction in drag with thickness ratio, a fair comparison between the original and designed body should really be performed with both at the same thickness. The drag of the rescaled redesign is obtained using the transonic similarity rule, which for axisymmetric bodies of thickness ratio δ is

$$\tilde{C}_D \equiv \frac{C_D}{\delta^4} = f(K'), \tag{31a}$$

where

$$K' = (1-M_\infty^2)/\delta^2. \tag{31b}$$

Accordingly, if a C_{D_1} is associated with an $R_{1_{MAX}} = \mu$, and $\mu<1$, say, then the body thickness ratio should be increased by a factor μ^{-1}, and a new drag coefficient C_{D_2} should be calculated from a new analysis solution to evaluate $f(K_2')$, where $K_2' = \mu^2 K_1'$. Then

$$C_{D_2} = \frac{1}{\mu^4} f(\mu^2 K_1'), \tag{32}$$

is the appropriate comparison drag coefficient for the blown-up redesigned body. Since the rescaling of K_1' to $\mu^2 K_1'$ drastically changes the flow field,

with a probable generation or intensification of shocks for $\mu<1$, it is important to implement Step 7 in the PI procedure previously described if a meaningful drag reduction is to be achieved. Some results of preliminary efforts in this direction will be described subsequently. The procedure described in Ref. 9 embodies the feature of renormalizing R_{MAX} during its iteration cycle.

As a basis of a different sort of standardized comparison, the flow field over a reference parabolic arc body with $R_{MAX} = .524$ was computed at $K = 1.48$, the value utilized for the original parabolic and the redesigned body. By contrast to the redesigned body, a surface shock was exhibited for the parabolic body, although the drag was still low ($C_D = .00066$), but three times larger than the redesigned body.

Since the emphasis in the PI method is to achieve closure as well as address the question of the existence of drag-free bodies at transonic speeds, the issue of R_{MAX} standardization is of lesser importance at this stage of the discussion. The significance of the redesign of Fig. 7 can be more fully appreciated from a picture of the flow above the body. These are shown in what follows in terms of isobar and isoMach level lines. In Fig. 10, the isobar pattern for the parabolic reference body at the conditions of Fig. 7 are indicated. The solid lines indicate expansion regions and the dashed lines signify compressions. Evident in the map is the concentration of contours above the 75% location of the body associated with the shock. A corresponding isoMach map is shown in Fig. 11, where the supersonic bubble is shown, as well as the transition from supersonic to subsonic flow at the shock.

By contrast to the shocked pattern evident in Figs. 10 and 11, Figs. 12 and 13 indicate a shock-free mixed flow. Thus, in spite of the R_{MAX} reduction, these figures provide some insight into the issue raised previously regarding whether drag-free bodies of revolution exist in mixed flow. On the basis of the apparent shock-free nature of the flow field and the extremely low drag value $C_D = .00022$, prospects would appear

SC82-16845

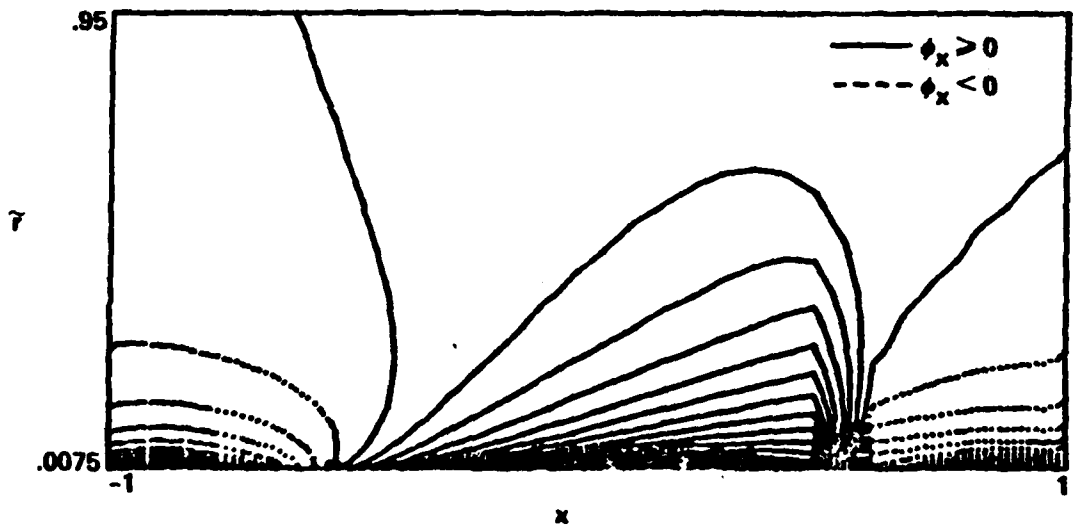

Fig. 10. Isobar map for parabolic reference body

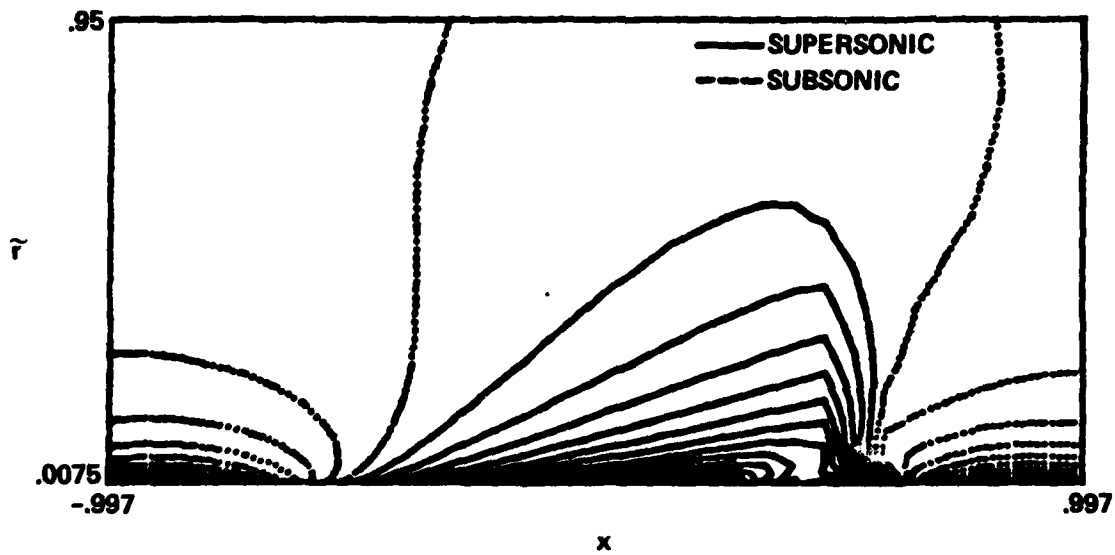

Fig. 11. IsoMachs - parabolic body of Fig. 7

SC82-16846

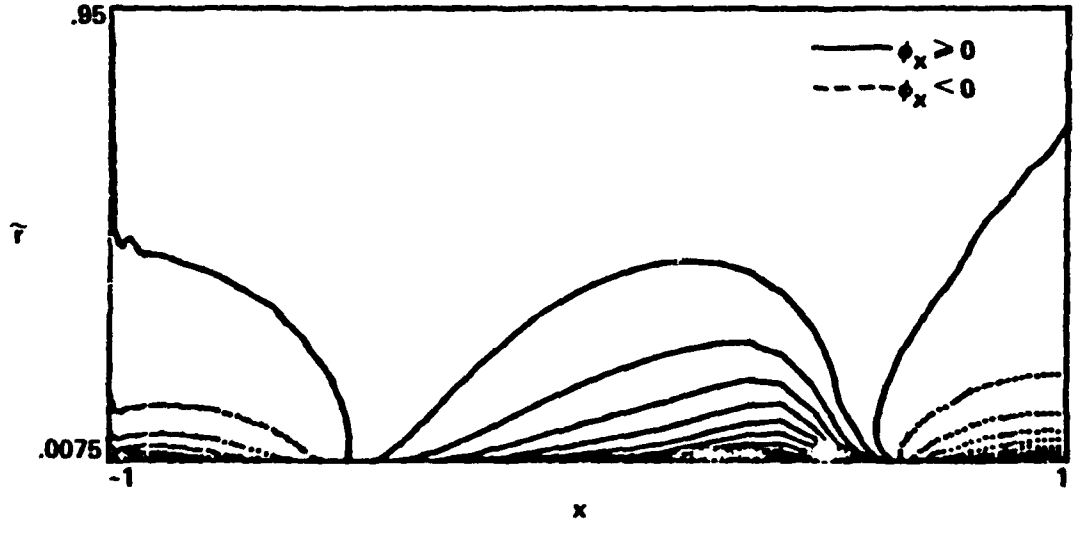

Fig. 12. Isobar map for redesigned body

SC82-16848

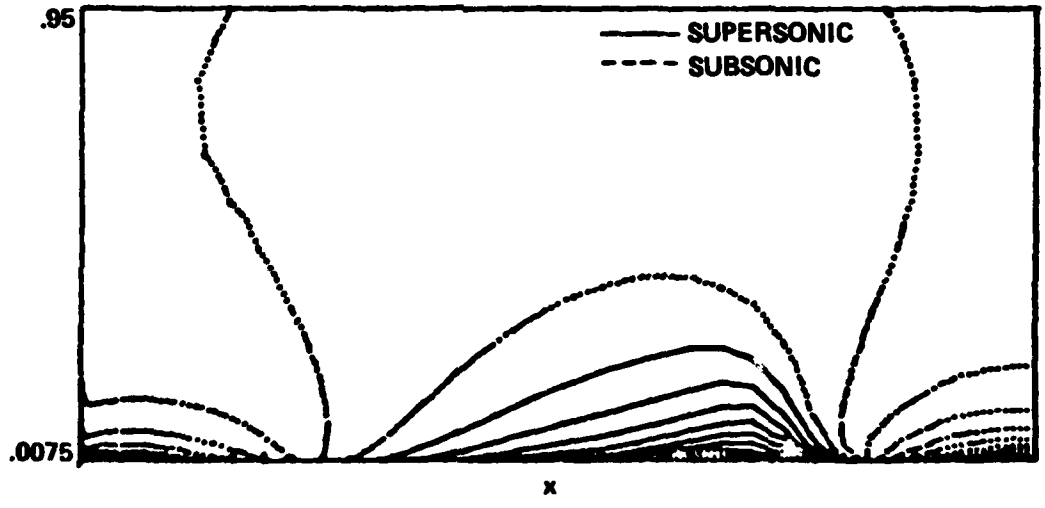

Fig. 13. IsoMachs - redesigned body, (height of sonic bubble ≈ .24)

encouraging for finding such bodies. The PI method appears to provide an attractive procedure to generate such shapes that close. To further elucidate the drag controlling mechanisms relevant to this evidence, the nonlinear axisymmetric hodograph should receive attention. In two-dimensional airfoil flows, the hodograph is linear, Garabedian solves it numerically, and Nieuwland provides analytical solutions. In some sense, these treatments prove the existence of shock-free airfoils. Due to the nonlinearity of the hodograph for the axisymmetric case, existence of shock-free bodies can probably only be demonstrated in a constructive sense, i.e., the numerical solution of the boundary value problem in the hodograph plane.

It is also interesting to note that Fig. 7, shows that the point of maximum thickness moves rearward for drag reduction in mixed flow over a body. This is in agreement with the optimum supersonic airfoil, which is a vertically symmetric wedge section, whose maximum thickness moves aft with increasing Mach number.

Returning to Fig. 5, a study of the sensitivity of the drag due to the fairing parameter a was conducted. The results are shown in Fig. 14, where C_D and R_{MAX} are plotted versus -a. A systematic trend is indicated showing that potent gains can be achieved through the use of relatively simple minded smoothings of the shock discontinuities.

In a previous treatment of the optimization problem for bodies of revolution, Chan[10] treated a two-parameter family of general parabolic bodies of the form $S(x) = Ax^n(1-x)^m$, $A = (n+m)^{(n+m)}/8n^n m^m$ using "numerical optimization" to determine the best selection of n and m to minimize the drag. As in most optimization procedures, the best selection of n and m did not eliminate the drag, and provided only a local extremum. In the PI procedure, there appears to be an opportunity to control the drag directly, through the shock smoothing mechanism mentioned previously.

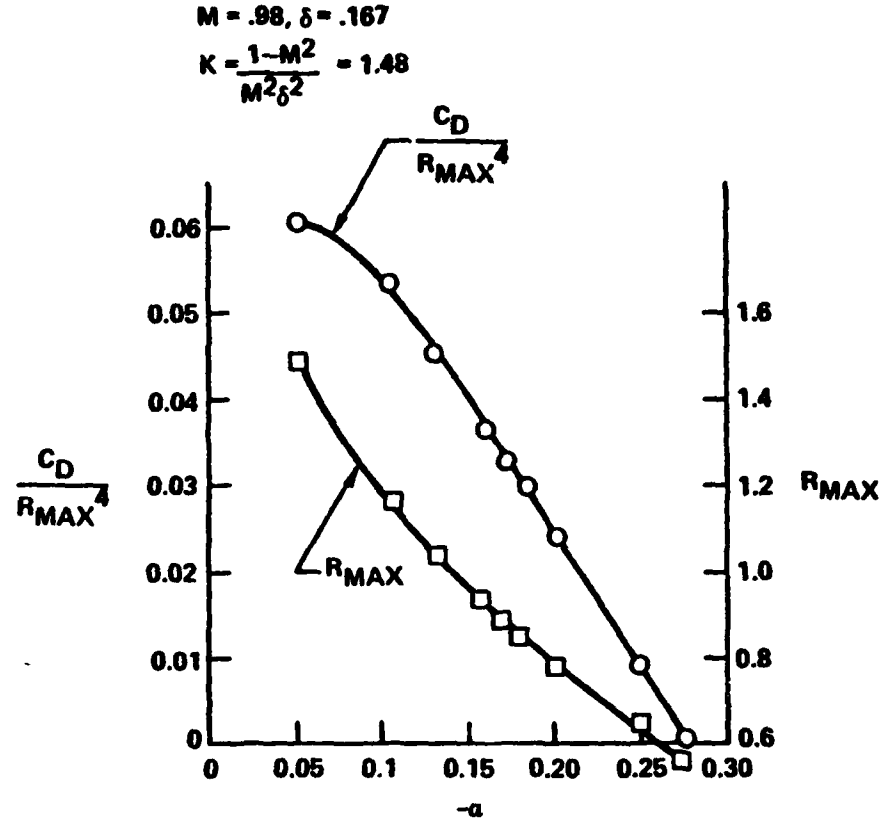

Fig. 14. Wave drag and EBR maximum thickness R_{MAX} versus surface C_p smoothing parameter, a

Another study of wave drag associated with various values of the parameter a is shown in Fig. 15, where the entropy jump integral across the shock which is proportional to the wave drag is shown. Dramatic differences are shown, in which a fairing parameter a = -.109 can be selected to give a drag actually higher than that of the parabolic body. Also indicated is a very small value associated with a = -.2. In the figure, the irregularities indicated are associated with the usual difficulties of shock capture.

In the study of the optimization process, a question of significance arises concerning whether the parabolic body is a disadvantageous initial iterate for PI process. The thrust of the question pertains to the possibility that flattened bodies such as supercritical airfoils are useful as drag reducers, since their slope contributions to the wave drag integral are nearly zero on their nearly cylindrical portions. The associated shocks could also be weak due to suppression of the envelope of the reflections. One candidate for consideration is the shape shown in Fig. 16 hereinafter referred to as the tanh body. In spite of the deleterious effect of overexpansions near the forebody shoulder and the resulting shock, the drag can be minimized to about 1/2 of the parabolic value through the selection of the parameter ϵ, the effective forebody length. It is interesting to note that $\epsilon = 0.12$ gives about three times the parabolic body result for the tanh shape.

As an illustration of some of the nonlinear wave steepening mechanisms present, Fig. 17 shows a sequence of axial distributions of pressure at various heights above the body. The results are plotted for the minimum drag value of ϵ. The impossibility of improvement stems from overtaking of the expansion-compression hump over the afterbody shoulder by another hump from the forebody shoulder. As the height increases, the latter swallows up the former. At even greater heights, a mild shock forms. The shock was detected in this case by monitoring finite jump discontinuities of ϕ_{xx} and using expanded scales in graphic visualizations of the process.

SC82-16849

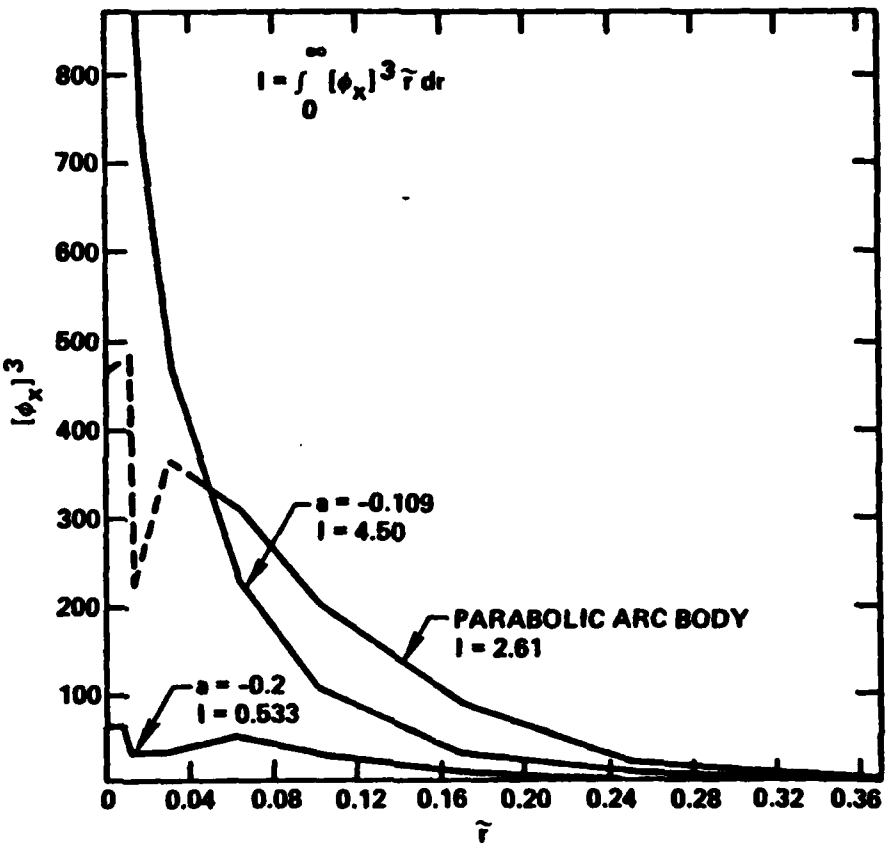

Fig. 15. Entropy jump shock drag for various bodies

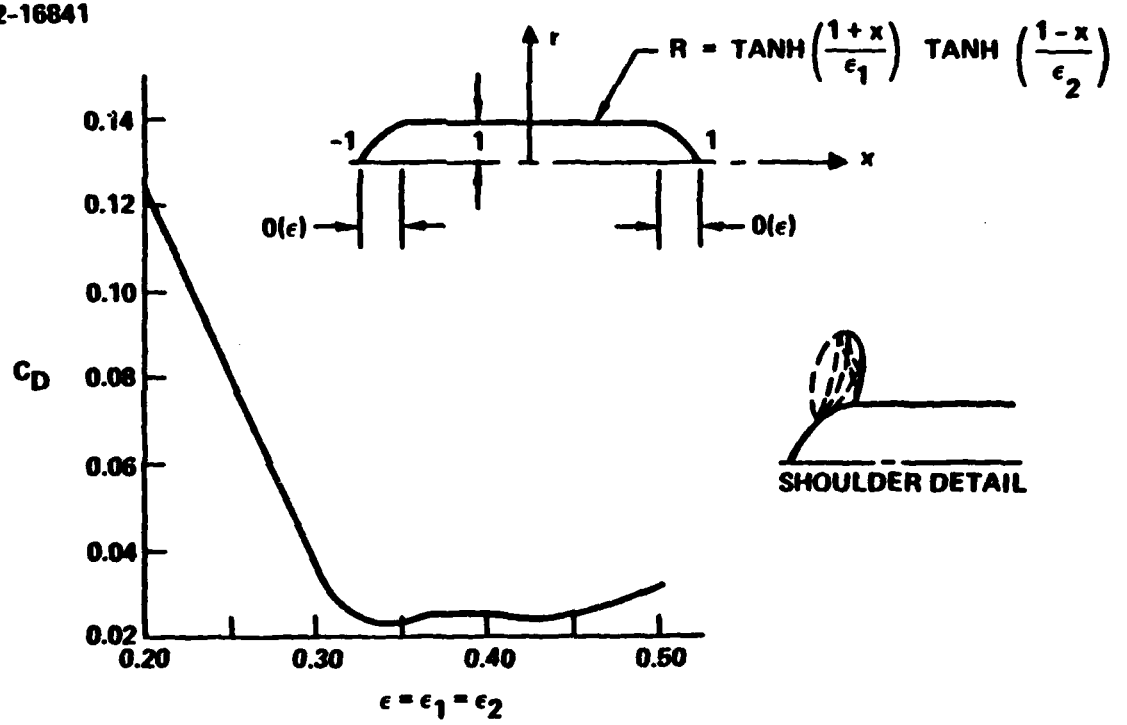

Fig. 16. Wave drag of nearly cylindrical bodies

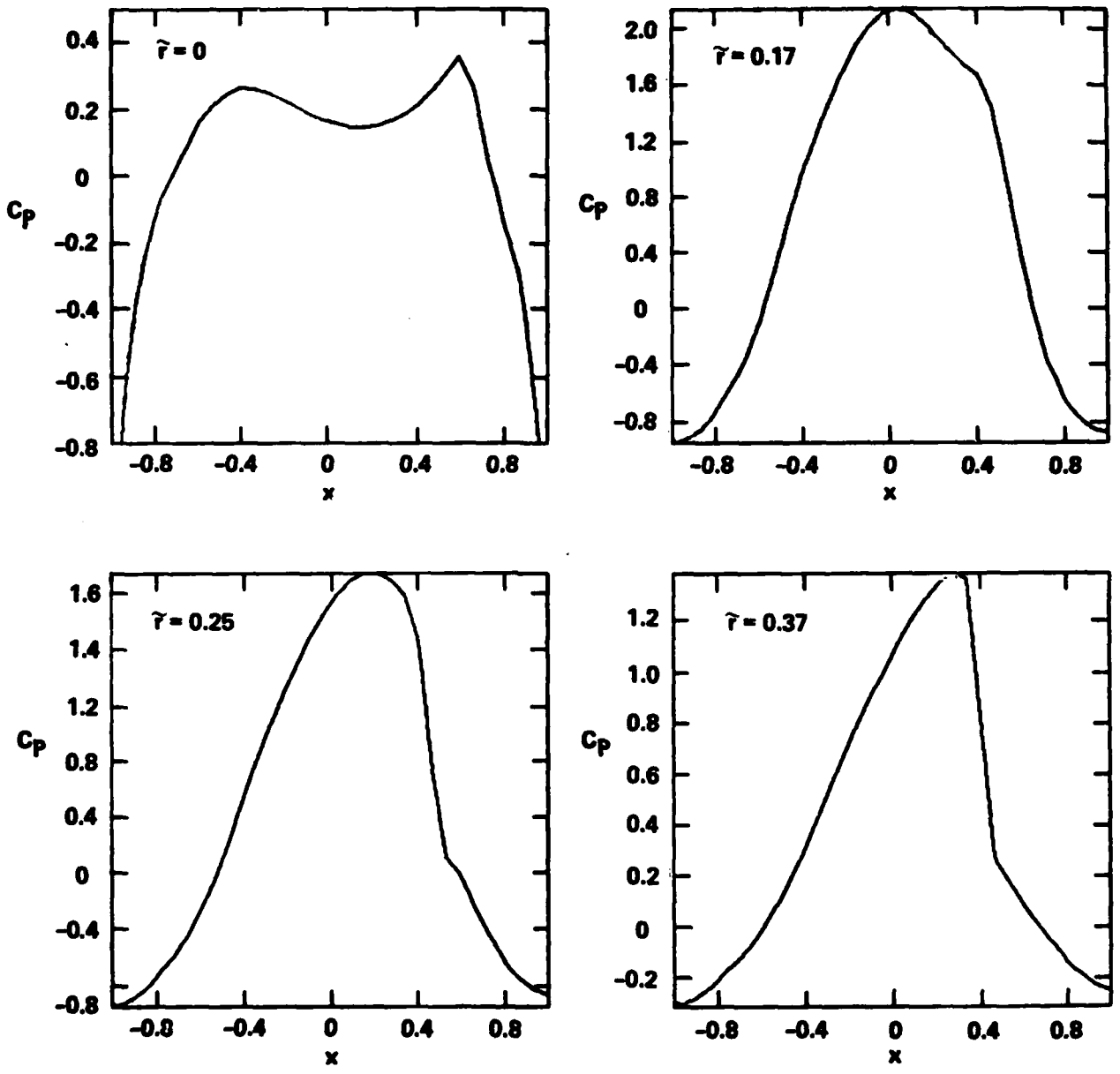

Fig. 17. Development of C_p vs. x at various levels above tanh body

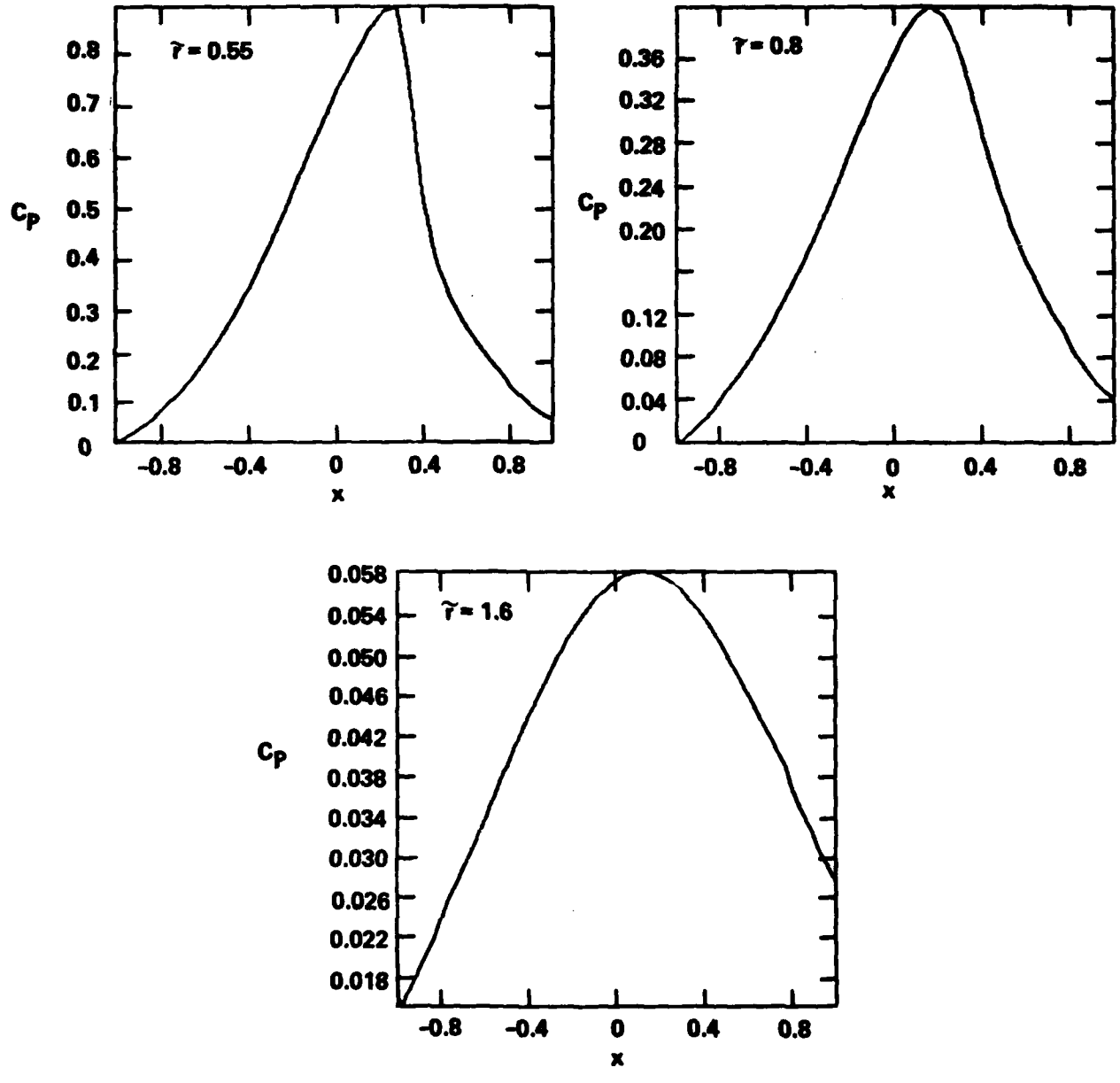

Fig. 17 (cont'd) Development of C_p vs. x at various levels above tanh body

To demonstrate the implementation of Step 7 in the PI method, the case of Fig. 7 was run again in which the parameter a = -0.17. In Fig. 18, the body solution is shown as the indicated bulge about the parabolic contour. Fig. 19 indicates the redesigned pressure distribution associated with the bulged contour. It should be noted that spikes are due to limited convergence of the iterations for this case. Part of the marginality of convergence stems from possible existence and nonexistence of neighboring solutions in the iteration space. However, these difficulties are deemed to be solvable with further numerical experimentation. The axial distributions of pressure at various heights above the body have the same steepening characteristics that are indicated in Fig. 17.

The important point about the cases in Figs. 17 and 18 is that they conclusively demonstrate that smoothing on the body may not always eliminate wave drag or shocks off the body. Therefore, the envelope formation process should be studied carefully in future effort.

In connection with earlier remarks on L/D, the last example shown in Fig. 20 illustrates the use of the PI procedure for a constrained finite base. As usual, the reference parabola is indicated for comparison purposes. The associated refaired pressure distribution is indicated in Fig. 21. For this case, the maximum velocity potential differences between old and new solutions near the end of the iteration sequence employed were as follows:

$$\left.\begin{matrix}\text{Analysis} \\ \text{Loop}\end{matrix}\right\} : \text{Max}\ (\phi^{n+1} - \phi^{n}) = 0.0003$$

$$\left.\begin{matrix}\text{Design} \\ \text{Loop}\end{matrix}\right\} : \text{Max}\ (\phi^{n+1} - \phi^{n}) = 0.00815$$

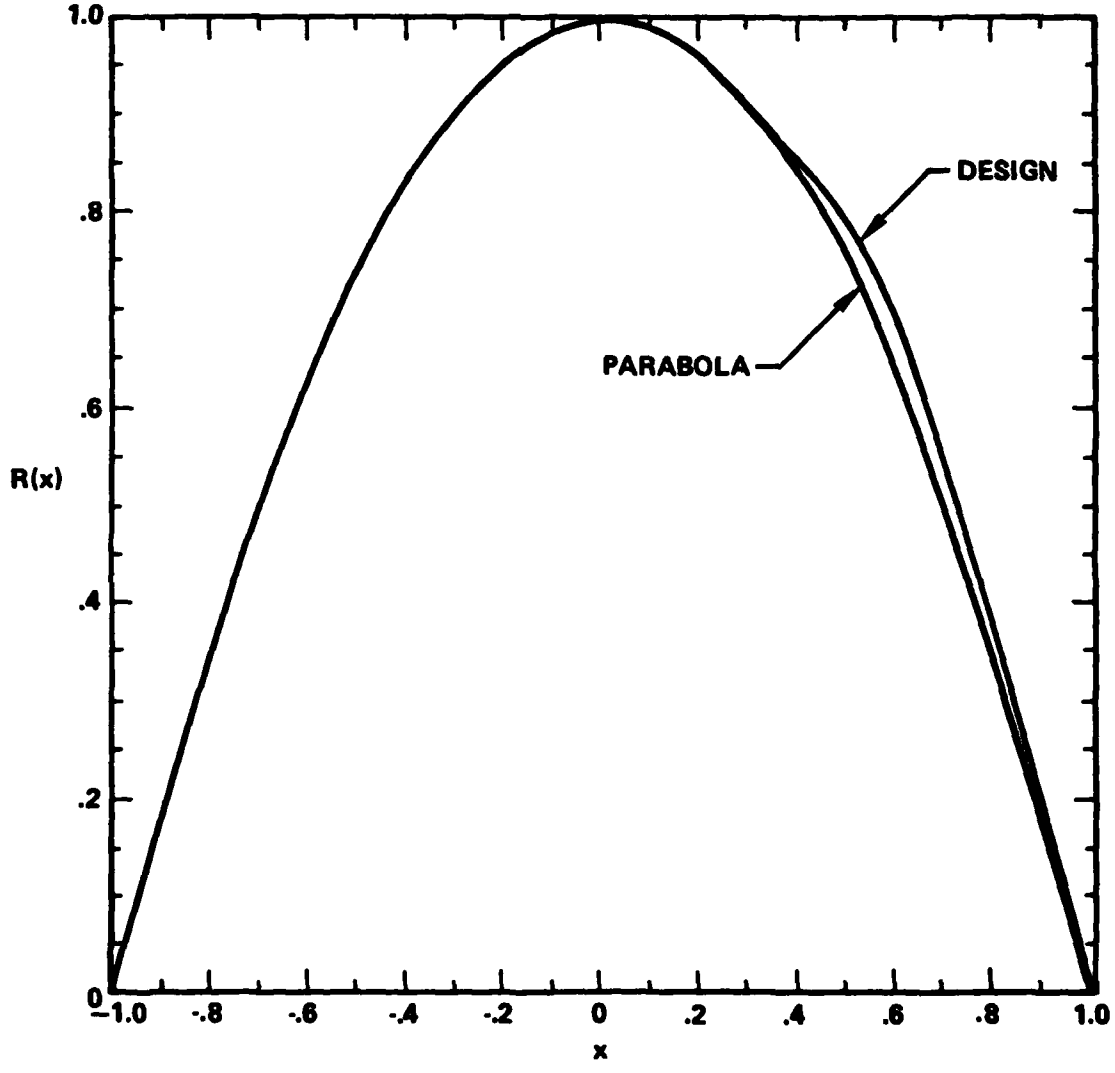

Fig. 18. Body design with R_{MAX} = 1 constraint and closure implemented M_∞ = 0.98, δ = 0.167

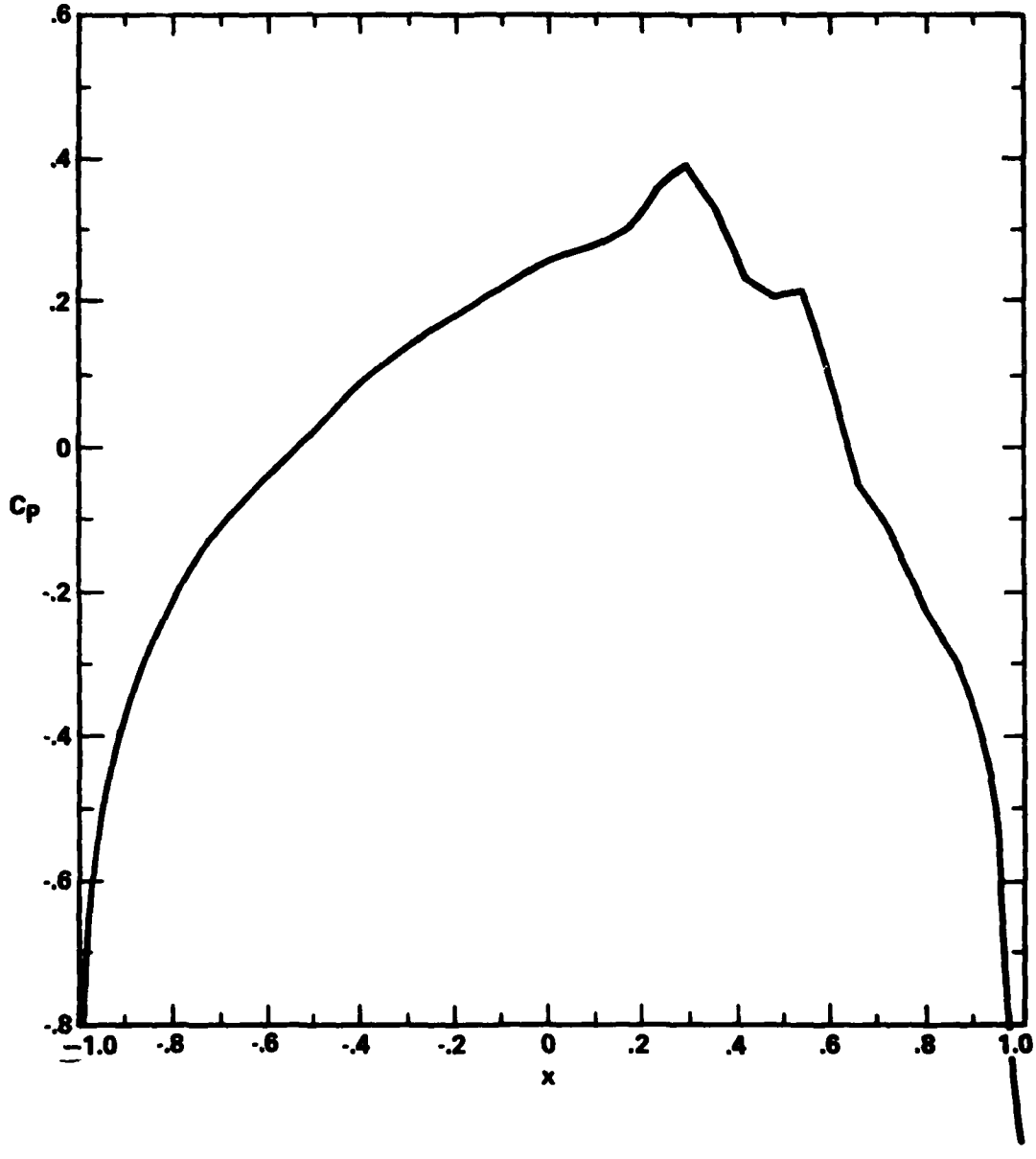

Fig. 19. Pressure distribution (partially converged) for redesigned body with $R_{MAX} = 1$, case of Fig. 18

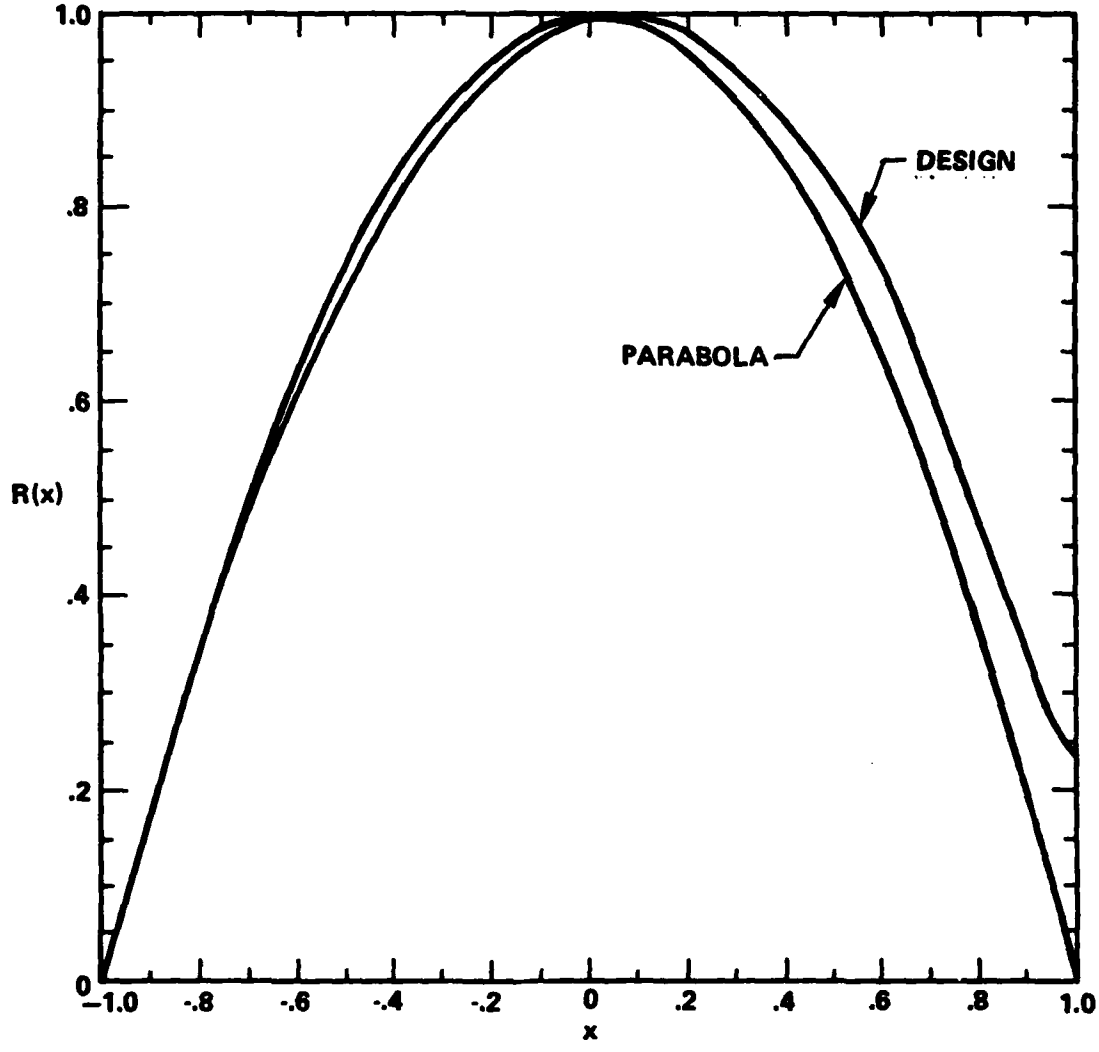

Fig. 20. Body design with a constrained finite base, parameters identical to Fig. 18

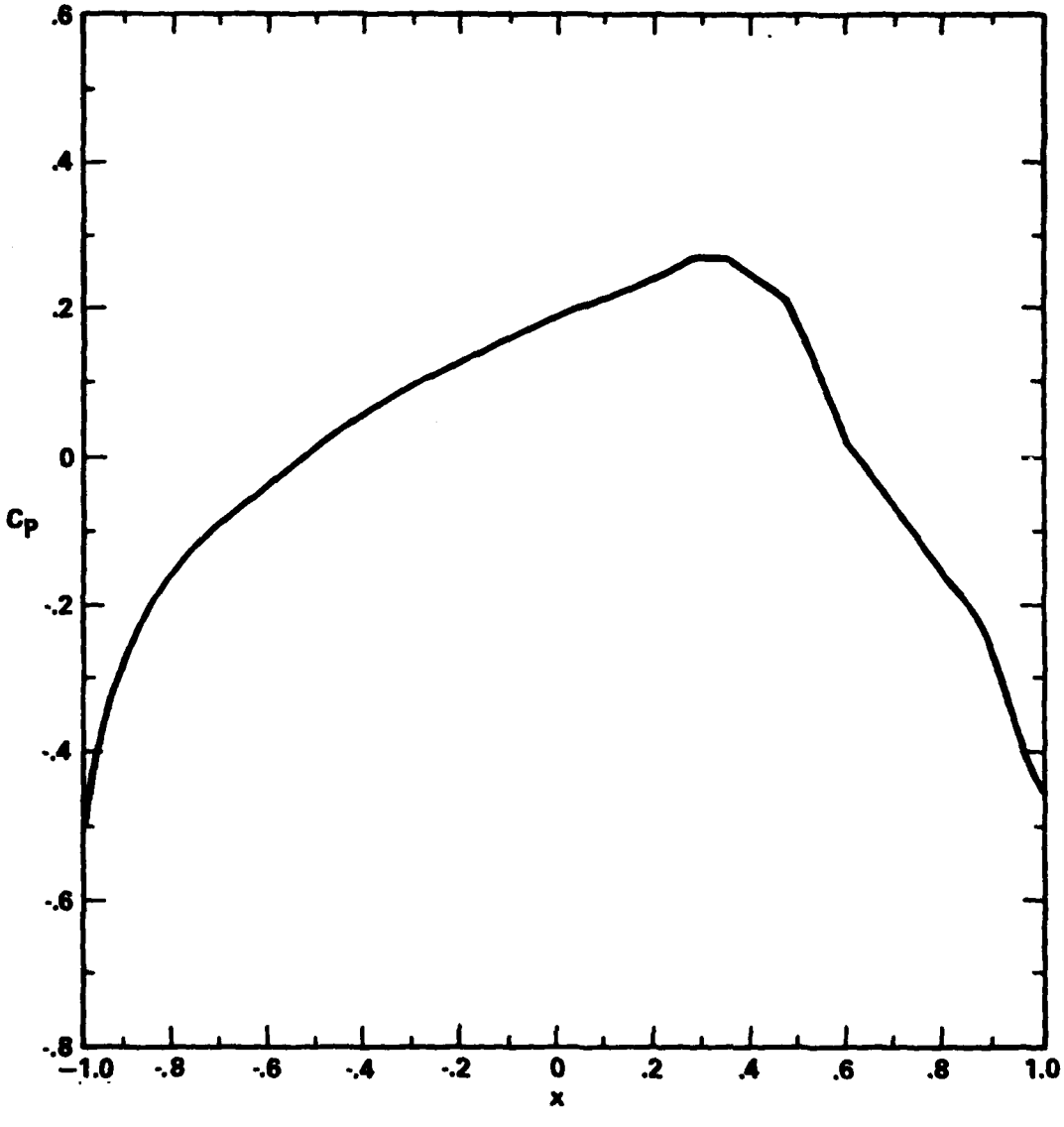

Fig. 21. Redesigned pressure distribution for case of Fig. 20

The convergence rate of the second difference was slow, but the impact of this behavior appears to be small on the difference between the actual value of C_p obtained and the target variation. In Table 1, a comparison of the constrained R_{MAX} and R_{BASE} cases is shown. Drag levels are also indicated against the parabola value.

TABLE 1. COMPARISON OF DRAGS - OPTIMIZED CONSTRAINED BODIES AGAINST PARABOLIC TYPE

Run	a	R_{BASE}	R_{MAX}	C_D	C_D/R^4_{MAX}
90A	-0.17	0.2	0.841	0.0130	0.026
90B	-0.17	0	1	0.0384	0.0384
PARABOLA	-	0	1	0.0459	0.0459

It is evident from the table that substantial improvement from the drag level of the parabolic body was made with the constrained maximum thickness generalization of the PI procedure. In the implementation for the finite base case, the absence of the tail singularity was ignored, with no major effect on the convergence of the closure iteration loop. Worthy of mention in this connection is the subtle distinction between a sting support, open body, wake and finite base. For the first, second and fourth situations, a tail singularity is possible, whereas for the third, it is unlikely.

4.0 CONCLUSIONS

In the previous sections, results of our research on transonic slender body theory toward obtaining an unsteady equivalence rule and application of an axisymmetric inverse design method to the study of nonlinear area ruling concepts have been presented. Asymmetric configurations were considered in the research. For certain classes of these shapes in which the wing is of zero thickness and increases its span montonically from a common apex, the L/D optimization problem consists of minimizing the drag of the body for a fixed span of the wing. Furthermore, if the body is pointed, the wing-body interference lift has been shown by previous investigators to be that of the isolated wing. For the drag minimization process for these lifting wing body combinations, it is clear now that the PI method developed during the research program can provide an extremely useful tool.

Substantial reductions of the wave drag can be achieved in many cases in which the surface pressure jump discontinuity is refaired. It has been also demonstrated that the refairing process can be utilized to achieve satisfaction of constraints such as closure and fixed maximum thickness. However, there are certain situations in which shocks develop off the body. These have been demonstrated in our effort. For these cases, the elimination of a surface discontinuity may reduce the wave drag but not completely eliminate it. Therefore, a knowledge of the theory of characteristic propagation and envelope formation for flow over axisymmetric bodies could provide target surface pressures to eliminate these off-body shocks. Other aspects of the research have shown that the initial iterate in the design process can play a role in the degree of drag minimization that is possible. In fact, a study of a nearly cylindrical body when optimized in its forebody and afterbody sections provides substantial reductions from the symmetric parabolic shape, if the lengths of these sections are optimized. The role of overexpansions and shock formation is intimately involved in the proper adjustment of these lengths as has been previously discussed.

One question answered by the research effort concerns the existence of shock-free flow over axisymmetric shapes. From the results, it would appear that to within the truncation errors of the numerical methods, the answer must be in the affirmative. Because of the limited information available however, more cases should be investigated and the existence question should be studied by other methods such as the axisymmetric hodograph.

For unsteady flows, analytical results have been provided that indicate the existence of an unsteady equivalence rule. Just as in the steady case, the three-dimensional nonlinear problem for slender shapes can be simplified to an axisymmetric one, with internal boundary conditions associated with asymptotic behavior of an inner solution which is harmonic in cross planes. With the substantial current cost of computing transonic unsteady flows, as well as the need for avoiding non-classical flutter, the simplifications and cost reductions afforded by such a rule could be of substantial advantage.

5.0 RECOMMENDATIONS

On the basis of the previous findings, it is evident that slender body theory may be exploited with modern computational techniques to provide a basis for design synthesis of three-dimensional fighter and missile configurations. Current practice in many organizations is to use a linear "base point" and optimize on a trial and error basis from direct solvers, inverse methods applied to an isolated component such as a wing, or wind tunnel tests. Because this may result in a suboptimal extremum prejudiced by the linear base point, an alternate procedure is needed. For this purpose, the PI method described in this report appears attractive. However, for this tool to be more useful, additional development is required along the following lines:

1. Wings of zero thickness in combination with circular arc-cross section bodies were investigated. Although providing an indication of the significance of wing body interactions as they relate to appropriate directions for gains, the issues of wing thickness and body asymmetries should be addressed. For such generalizations, an involved tradeoff becomes evident between exposed area, for lift and nonlinear area ruling required to reduce the wave drag. An associated challenge is related to the ability to "unfold" the optimum equivalent body of revolution determined by the PI method to produce optimum compromises of design attributes such as those between aerodynamic efficiency and volume.

2. Another aspect of significance in the optimization process deals with the interaction of wakes associated with planforms of non-montonically increasing span in the downstream direction. The implication of these effects on the equivalence rule and the optimization procedures considered here

should be considered in future work. Propulsive effects such as jets emanating from the base are other possible avenues of research in which streamwise interactions are of importance. Effort should be expended on the exploitation of these effects for beneficial interference.

3. On a more fundamental basis, the theory of characteristic propagation should be utilized to shed light on envelope, focusing and caustic phenomena associated with shock wave development off axisymmetric bodies, particularly when no surface discontinuities are encountered as in the examples described in previous sections. This information could be used to suggest the types of faired pressure distributions leading to zero wave drag. Although we have demonstrated encouraging evidence regarding the existence of shock-free axisymmetric shapes, more information is needed on how they can be produced from the PI method.

4. The work previously described considered iterative procedures to satisfy various constraints. More effort is required to handle generalized situations involving prescribed volume, surface area, and multiple design points. From this standpoint, viscous effects for example such as those dealing with friction drag, adverse pressure gradients, are all areas that are of interest.

5. For both the steady and unsteady problems, the materialization of shocks in the near field as well as special asymptotic boundary layers required to treat these structures are of interest regarding matching in higher orders of the slender body theory. These aspects are important with respect to nonlinear lift corrections in the slender body theory, and studies of the impact of lift on the equivalence rule as described in Refs. 11 and 12.

6.0 REFERENCES

1. Whitcomb, R.T., "A Study of the Zero Lift Drag Rise Characteristics of Wing-Body Combinations Near the Speed of Sound," NACA Report 1273 (1956).

2. Oswatitsch, K., and Keune, F., "Ein Äquivalensatz fur Nichtangestellte Fluge Kleiner Spannweite in Schallnaher Strömung, "Zeitschrift fur Flugwissenshaften 3 Jahrgung Heft 2, February 1955, S. 29-46.

3. Heaslet, M.A., and Spreiter, J.R., Three-Dimensional Transonic Flow Theory Applied to Slender Wings and Bodies, NACA Report 1318, 1956.

4. Shankar, V., Malmuth, N.D., and Cole, J.D., "Computational Transonic Inverse Procedure for Wing Design, "AIAA Paper 80-1390 presented at the AIAA 13th Fluid and Plasma Dynamics Conference, Snowmass, Colorado, July 14-16, 1980, to appear in AIAA J. August 1982.

5. Cole, J.D., "Studies in Transonic Flow I, Transonic Area Rule - Bodies," UCLA Rpt., UCLS-Eng. 7257, August 1972.

6. Cole, J.D., "Studies in Transonic Flow IV - Unsteady Transonic Flow," UCLA Rpt., UCLA-Eng. 76104, October 1976.

7. Krupp, J.A., and Murman, E.M., "Computation of Transonic Flows Past Lifting Airfoils and Slender Bodies," AIAA J.

8. Ashley, H., and Landahl, M., Aerodynamics of Wings and Bodies, Addison-Wesley, Reading, Mass., 1965.

9. Shankar, V., "Numerical Boundary Condition for the Transonic Axisymmetric Inverse Problem," Proceedings of Symposium on Numerical Boundary Conditions Procedures, October 19-20, 1981, NASA CP2201, 1982, pp. 183-197.

10. Chan, Y.Y., Mundie, D.L., and Jones, D.J., "Transonic Axisymmetric Bodies with Minimal Wave Drag," Canadian Aero. and Space J., 26, 3, 1980.

11. Cheng, H.K., and Hafez, M.M., "Transonic Equivalence Rule; a Nonlinear Problem Involving Lift," J. Fluid Mech., 72, pt. 1, 1975, pp. 161-187.

12. Barnwell, R.W., "Transonic Flow About Lifting Configurations," AIAA J., 11, May 1973, pp. 764-766.

PART 2

ASYMPTOTIC THEORY OF SOLID TUNNEL WALL INTERFERENCE ON TRANSONIC AIRFOILS*

SUMMARY

The method of matched asymptotic expansions is utilized to study the singular perturbation problem of solid wall interference on transonic airfoils. For moderate to large wall heights, the (inner) near field is represented as a linear perturbation about the nonlinear free field which is assumed to be governed by the Karman-Guderley small disturbance theory which is non-uniformly valid as the walls are approached. In the far field (outer) region, another approximate representation of the wall-airfoil interaction involving a multipole, dominated by a vortex reflected between the walls is valid. Through the use of intermediate limits, matching of both representations is demonstrated. Some numerical solutions for the inner problem are illustrated in which the inner limit of the outer solution is employed as a far field boundary condition for the perturbed flow. Means of correcting the tunnel incidence to obtain an interference-free value for the lift are demonstrated from the examples. By virtue of the nature of the perturbation method, the height dependence is separated out from the problem and universal correction functions are available from the theory for airfoils at given incidence and Mach number conditions.

*To be presented as AIAA paper 82-0933 at the AIAA/ASME 3rd Joint Thermophysics, Fluids, Plasma and Heat Transfer Conference June 7-11, 1982/ St. Louis, Missouri.

1.0 INTRODUCTION

Obtaining free-field characteristics of transonic wind tunnel models will continue to be of central importance to aeronautical technology for the indefinite future. Free flight aircraft performance predictions depend on this process which is complicated by the presence of complex nonlinear phenomena in the transonic regime. Although the wind tunnel interference problem has received considerable attention at subsonic speeds, and a number of classical theories have been developed, e.g., Refs. 1-3, there is room for progress even in this linear regime, as exemplified by the recent efforts of Kraft,[4] who devised an ingenious procedure based on Cauchy's integral formula for two-dimensional flow over confined airfoils. Among the advantages of this method in contrast to the older concepts is that by measurement of two flow variables it eliminates the need for both knowledge of the wall characteristics and analytical synthesis of the model. Presently, effort is underway to extend this procedure to three-dimensional and nonlinear transonic flows.

In connection with the transonic regime, other procedures have been developed which possess attractive features. One, which is of great interest, is a scheme that has been developed by Murman. This "post test assessment method", which has been implemented in two-dimensions in Ref. 5, is similar in some respects to an approach developed earlier by Kemp,[6] and assumes a knowledge of the experimental pressures on the model and walls. It uses modern computational and optimization procedures to determine whether the tunnel Mach number and model angle of attack are correctable in the sense that almost free-field model pressures can be obtained at practically altered values of these parameters. For this purpose, an inverse problem needs to be solved. In three-dimensions, surface pressures over the model are generally not available, and efforts are currently under way to modify the method toward the use of less information regarding the model near-field.[7] If this goal can be achieved, this process will be of value, including treatment of cases in which the walls are relatively

close to the model. In spite of the potential utility of this method, there is a need for approaches that can reduce the number of input parameters necessary to compute the correction, shed light on the physics of the wall interference phenomena, simplify the necessary computations, and be generalized to three-dimensions, as well as unsteady flows. Asymtotic procedures provide such advantages. Furthermore, they can provide valuable interactions with the other methods previously mentioned to suggest possible improvements as well as deriving beneficial features from them as well.

In this report, an application of the asymptotic method to the two-dimensional case involving a transonic airfoil between solid walls will be studied. This effort is a forerunner of three-dimensional formulations which besides their own intrinsic utility have relevance to the methods of Ref. 4 and 5. Regarding the latter, one concept presently being considered to simplify its three-dimensional application is unfolding the singular character of the near-field rather than obtaining the model's shape from an inverse solution of a problem involving specified pressures based on measured values. As will be evident from what follows, the asymptotic procedures can provide this singular behavior from certain limit processes. Moreover, nonlinear integral theorems as well as the asymptotic structure of nonlinear integral equations arising in the matching scheme occurring in the asymptotic analysis could be of use in the procedure of Ref. 4.

Whereas methods such as those of Refs. 1-7, can handle arbitrary model to wall dimension ratios ϵ, the perturbation procedure assumes ϵ to be small. This approximation is useful for many practical cases. Furthermore, even for situations where ϵ is not so small, the expansions appear to have extended validity.

A previous analysis along these lines was conducted by Chan[8] who treated the two-dimensional porous wall case. Because of its interest in connection with compliant boundary applications and the fact that the

Chan solutions apparently do not subsume it as might be expected by a taking a limit of the porosity parameter, we analyze the solid wall case in this report. By contrast to the method of Ref. 8, we employ "intermediate variables" to match the model near and far fields. Although slightly more cumbersome than the approach utilized by Van Dyke,[9] we believe it provides a reliable means of ensuring that all the proper terms are included in both representations.

In addition, numerical results will be provided in the report to give some insight into the nature and magnitude of the interference effects. The work of Ref. 8 in this sense was strictly formulation, with no computational application or quantification of the interference given.

2.0 ANALYSIS

Referring to Fig. 1, which indicates an airfoil nearly midway between solid walls, in which $\tilde{y} = y\delta^{1/3}$, x and y are Cartesian coordinates in units of the chord, h is the tunnel half height in the same units, U_T and M_T are respectively free-stream speed and Mach number in the tunnel, and transonic flow conditions are assumed in accord with a Karman Guderely (KG) limit. Thus, if δ is a characteristic thickness ratio of the airfoil whose shape is given by

$$y = \delta F_{u,\ell}(x) - \alpha_T x, \quad |F_{u,\ell_{MAX}}| = 1 \tag{1}$$

where the thickness ratio is considered as unvarying from the (unbounded) free field* and subscripts u and ℓ denotes upper and lower surfaces and α_T is the angle of attack in the tunnel, the appropriate expansion for the velocity potential is

$$\Phi = U_T \left\{ x + \delta^{2/3} \phi(x, \tilde{y}; K_T, A_T, H) + \ldots \right\} \tag{2a}$$

which is valid in the KG limit

$$x, \tilde{y}, \; K_T = \frac{1-M_T^2}{\delta^{2/3}}, \; A = \frac{\alpha_T}{\delta}, \; H = h\delta^{1/3} \quad \text{fixed as } \delta \to 0, \tag{2b}$$

*More general situations could be considered.

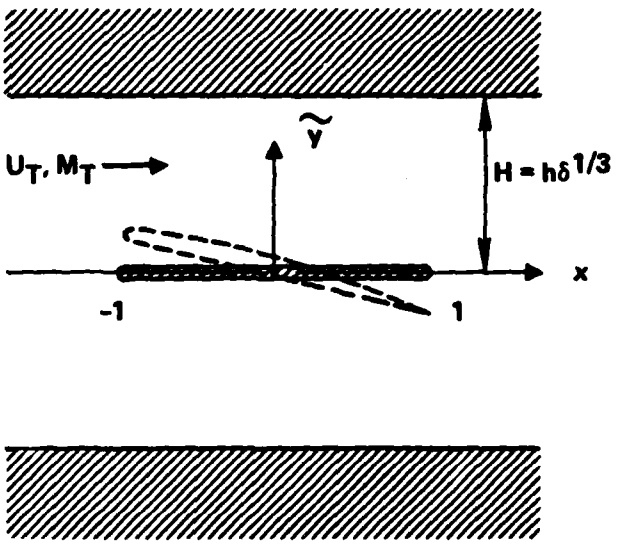

Fig. 1. Confined airfoil

and leads to the following small disturbance problem* for the confined transonic airfoil:

$$[K_T - (\gamma+1)\phi_x]\,\phi_{xx} + \phi_{\tilde{y}\tilde{y}} = 0 \tag{3a}$$

$$\phi_{\tilde{y}}(x,0\pm) = F_{u,\ell}'(x) - A_T \tag{3b}$$

$$\phi_{\tilde{y}}(x,H\pm) = 0 \tag{3c}$$

$$[\phi_x]_{\substack{TE \\ (x=1)}} = 0, \text{ Kutta-Joukowski Condition} \tag{3d}$$

2.1 Inner Problem

A simplification of the problem associated with Eqs. (3) can be considered in which expansions of ϕ in (2a) are considered for $H \to \infty$. Near the airfoil, the walls are remote and thereby introduce weak perturbations about a dominant nonlinear (KG) free field. Accordingly, an inner expansion is valid which can be written as

$$\phi = \phi_0(x,\tilde{y}) + \frac{1}{H^2}\,\phi_1(x,\tilde{y}) + \ldots \tag{4a}$$

$$x,\tilde{y} \text{ fixed as } (H = \epsilon^{-1}) \to \infty \text{ (inner limit)} \tag{4b}$$

in which subscript 0 denotes free flight and 1 is the dominant wall correction. The gauge function $\frac{1}{H^2}$ is anticipated as shown to achieve

*In the Results section this will be termed the "exact" problem.

asymptotic matching to be discussed subsequently. For generality and use in tunnel assessment and correction procedures, the similarity parameter and angle of attack are also written as perturbations about the free field values along with those for the potential in (4). Thus,

$$K_T = K_F + \frac{1}{H^2} K_C + \ldots \tag{5a}$$

$$A_T = A_F + \frac{1}{H^2} A_C + \ldots \tag{5b}$$

where subscripts F denote the free field, C is associated with wall corrections, and T designates the tunnel value. On substitution of (4) and (5) into the problem (3), and retaining corresponding orders, the zeroth and first order problems are obtained as

$$\left(K_F - (\gamma+1)\phi_{0_x}\right)\phi_{0_{xx}} + \phi_{0_{\tilde{y}\tilde{y}}} = 0 \tag{6a}$$

$$\left(K_F - (\gamma+1)\phi_{0_x}\right)\phi_{1_{xx}} - (\gamma+1)\phi_{1_x}\phi_{0_{xx}} + \phi_{1_{\tilde{y}\tilde{y}}} = -K_C\,\phi_{0_{xx}} \tag{6b}$$

$$\left.\begin{aligned} \phi_{1_{\tilde{y}}}(x,0\pm) &= F'_{u,\ell}(x) - A_F \qquad (6c)\\ \phi_{0_{\tilde{y}}}(x,0\pm) &= -A_C \qquad (6d) \end{aligned}\right\} \quad |x|<|$$

$$\left[\phi_{0_x}\right]_{TE} = \left[\phi_{1_x}\right]_{TE} = 0 \tag{6e}$$

In the problem associated with the "variational" equation (6b) which resembles others such as the lifting line theory of Ref. 10, the jumps across the 0^{th} order shocks are perturbed according to the developments given therein. In (6), if Γ is the circulation, it can also be written in the perturbation form

$$\Gamma_T = \Gamma_F + \frac{1}{H^2}\Gamma_C + \cdots \quad .$$

To complete the formulation, a far field is required. In this connection, it is crucial to note that the approximation (4a) is non-uniformly valid near the walls and an "outer" representation is required. An "inner" limit of this outer solution (approaching the boundaries of the airfoil near field) supplies the required inner far field boundary conditions. These will be discussed presently. For the far field of the 0^{th} order problem the representation,

$$\phi_0 = \frac{-\Gamma_F\theta}{2\pi} + \left(\frac{\Gamma_F}{2\pi}\right)^2 \frac{\gamma+1}{4K_F}\frac{\ell n\, r}{r}\cos\theta - \left(\frac{\Gamma_F}{2\pi}\right)^2 \frac{(\gamma+1)}{16K_F}\frac{\cos 3\theta}{r}$$

$$+ \frac{D_0}{2\pi}\frac{\cos\theta}{r} + \frac{E_0}{2\pi}\frac{\sin\theta}{r} \quad , \qquad (7a)$$

$$r = \sqrt{x^2 + K_F\tilde{y}^2} \to \infty \quad , \quad \theta = \tan^{-1}\frac{\sqrt{K_F}\tilde{y}}{x} \text{ fixed, (ray limit)} \qquad (7b)$$

is appropriate on the basis of Ref. 10. In addition, the far field anticipated and to be refined for ϕ_1 is

$$\phi_1 = B_1 x\tilde{y} + C_1 x + M_1 \tilde{y} + N_1 - \frac{\Gamma_C \theta}{2\pi} + \ldots \quad , \tag{7c}$$

in which $x^2, \tilde{y}^2$ quadratic terms are missing based on the matching to be indicated, and B_1, C_1, M_1 and N_1 are constants to be determined in this matching.

In this simulation, the aim is to select A_C and K_C to minimize the correction in some sense.

2.2 Outer Problem

At distances from the airfoil where the wall influence is not small, the outer expansions

$$\phi = \varphi_0(x^*,y^*) + \frac{\ell nH}{H}\varphi_{\frac{1}{2}}(x^*,y^*) + \frac{1}{H}\varphi_1(x^*,y^*) + \ldots \quad , \tag{8a}$$

are anticipated as valid in the limit

$$x^* = \frac{x}{H},\ y^* = \frac{\tilde{y}}{H} \text{ fixed as } H \to \infty, \text{ (outer limit)}, \tag{8b}$$

where the $\varphi_{\frac{1}{2}}$ "switchback" term is inserted, anticipating in the matching the effect of logs arising from the outer limit of (7a). On substitution in (3), the equations obtained for the terms in (8a) are

$$K_F \varphi_{0_{x^*x^*}} + \varphi_{0_{y^*y^*}} = 0 \quad , \quad O(1/H^2) \tag{9a}$$

$$K_F \varphi_{1_{x^*x^*}} + \varphi_{1_{y^*y^*}} = 0 \quad , \quad O(\ell nH/H^3) \tag{9b}$$

$$K_F \varphi_{1_{x^*x^*}} + \varphi_{1_{y^*y^*}} = (\gamma+1)\varphi_{0_{x^*}}\varphi_{0_{x^*x^*}}, O(1/H^3) \tag{9c}$$

with the wall boundary conditions,

$$\varphi_{0_{y^*}}(x^*,\pm 1) = \varphi_{1_{y^*}}(x^*,\pm 1) = \varphi_{1_{y^*}}(x^*,\pm 1) = 0. \tag{9d}$$

2.3 Preliminary Matching Considerations

Under the assumption that to dominant order, φ_0 is a potential vortex reflected between parallel walls, the exact expression from a Prandtl-Glauert scaled version of incompressible flow theory involving either images or conformal mapping is

$$\varphi_0 + i\psi_0 = F(Z) = \text{complex potential}$$

$$= \frac{i\Gamma_F}{2\pi} \ell n \tanh\left(\frac{\pi}{4}Z\right) \tag{10a}$$

$$Z = \frac{x^*}{\sqrt{K_F}} + iy^* \equiv X + iY \tag{10b}$$

The validity of Eqs. (10) is predicted on the assumption that the far field is subsonic. On expansion of (10) for $Z \to 0$, it is evident that

$$\varphi_0 = \frac{\Gamma_F}{2\pi}\left\{-\theta + \frac{\pi^2}{24\sqrt{K_F}}\, x^*y^* + \ldots\right\}, x^*,y^* \to 0 \ . \ (11) \qquad (11)$$

In (11), the x*y* term is the effect induced in the origin due to the wall reflections.

To compute φ_1, symmetry properties that can be inferred from the right hand side of (9c) are useful. These can be obtained from symmetries of φ_0 which are

$$\varphi_0(x^*,y^*) = -\varphi_0(x^*,-y^*)$$

$$\varphi_0(x^*,y^*) = -\varphi_0(-x^*,y^*)$$

from which it follows that

$$\varphi_1(x^*,y^*) = \varphi_1(x^*,-y^*)$$

$$\varphi_1(x^*,y^*) = -\varphi_1(-x^*,y^*)$$

With these relations in mind, the simular behavior required for matching can be obtained from a linear combination of particular, complementary, and homogeneous solutions of (9c), in which the complementary solution is added to satisfy the boundary conditions, and the homogeneous solutions are required to provide enough arbitrariness in the doublet strengths to achieve matching. Denoting φ_p as a particular solution, a choice is made for φ_p in which

$$\Delta\varphi_p = \frac{(\gamma+1)}{K_F^{3/2}}\varphi_{0_X}\varphi_{0_{XX}} = \frac{(\gamma+1)}{K_F^{3/2}}\psi_{0_Y}\psi_{0_{XY}}, \qquad (12)$$

where the right hand member of (12) is obtained from the Cauchy-Riemann equations and is used in favor of the middle one to avoid branch point singularities at the origin such as that occurring with the function $\Theta = \arg Z$, and ψ_0 is the harmonic conjugate of φ_0. Using a clever device employed in Ref. 11, the appropriate particular solution of (12) can be verified to be

$$\varphi_p = \frac{(\gamma+1)}{4K_F^{3/2}} \left\{ \psi_0 \psi_{0_X} + \gamma \psi_{0_X} \psi_{0_Y} \right\} \tag{13}$$

On expanding (13) near the origin Z=0, some of the necessary terms required for matching with (7a,c) appear, i.e.,

$$\varphi_p = \frac{(\gamma+1)}{4K_F} \left(\frac{\Gamma_F}{2\pi} \right)^2 \left\{ \frac{\ell n r^*}{r^*} \cos\theta - \frac{1}{4} \frac{\cos 3\theta}{r^*} + \left[\ell n \left(\frac{\pi}{4\sqrt{K_F}} \right) + \frac{1}{4} \right] \frac{\cos\theta}{r^*} \right.$$

$$\left. - \frac{\pi^2}{24} \frac{x^*}{K_F} \ell n r^* - \frac{\pi^2}{24} \frac{x^*}{K_F} \left(\ell n \frac{\pi}{4\sqrt{K_F}} \right) - \frac{\pi^2}{48} \frac{x^*}{K_F} \cos 2\theta + \ldots \right\} \tag{15a}$$

$$\text{as } r^* = \sqrt{x^{*2} + K_F y^{*2}} \equiv r/H \to 0 \tag{15b}$$

$$\theta^* = \tan^{-1} \frac{\sqrt{K_F}\, y^*}{x^*} = \tan^{-1} \frac{\sqrt{K_F}\, \tilde{y}}{x} = \theta, \text{ fixed.} \tag{15c}$$

The singular behavior of (14) near the origin contains no branches as desired. Consistent with earlier remarks, the appropriate doublet terms involving $\frac{\cos\theta}{r^*}$ are apparent and are of specific strength. However, additional ones of arbitrary adjustable strength are needed for matching. These will be obtained from a suitable homogeneous solution of (9c).

In view of these considerations, the complete solution of (9c) is written as

$$\varphi_1 = \varphi_p + \varphi_c + \varphi_h \tag{16}$$

where φ_c is a harmonic complementary solution added to satisfy the boundary conditions violated by φ_p. According to (9d),

$$\frac{\partial \varphi_c}{\partial Y}(X,\pm 1) = -\frac{\partial \varphi_p}{\partial Y}(X,\pm 1) = \mp \frac{(\gamma+1)}{4K_F^{3/2}}\left(\frac{\Gamma_F}{2\pi}\right)^2 \frac{\pi^3}{4} \frac{sh\pi X}{(1+ch\pi X)^2} \quad . \tag{17}$$

A Fourier integral representation for φ_c can be obtained from the wall source distribution $\frac{-\partial \varphi_p(X,\pm 1)}{\partial Y}$ in (17) as

$$\varphi_c = \frac{1}{\pi}\frac{(\gamma+1)}{4K_F^{3/2}}\left(\frac{\Gamma_F}{2\pi}\right)^2 \frac{\pi^3}{4} \int_0^\infty dk \int_{-\infty}^{\infty} \cos k(X-\xi) \frac{chkY}{kshk} \frac{sh\pi\xi}{(1+ch\pi\xi)^2} \, d\xi \quad ,$$

which upon integration simplifies to

$$\varphi_c = \frac{(\gamma+1)}{4K_F^{3/2}}\left(\frac{\Gamma_F}{2\pi}\right)^2 \frac{1}{2} \int_0^\infty \frac{\sin kX \; chkY}{sh^2 k} \, dk \quad .$$

The behavior of which as $X, Y \to 0$ is

$$\varphi_c \simeq \frac{(\gamma+1)}{4K_F}\left(\frac{\Gamma_F}{2\pi}\right)^2 \frac{\pi^2 x^*}{12} + \ldots \tag{18}$$

To obtain φ_H in (16), a further decomposition in which

$$\varphi_H = \varphi_S + \varphi_A + \varphi_{SC} + \varphi_{AC} \quad , \tag{19}$$

is used, where φ_S and φ_A are arbitrary strength doublets that are respectively symmetric and antisymmetric in y^* and φ_{SC} and φ_{AC} are complementary solutions added to each of these components to satisfy the wall boundary conditions. Thus,

$$\varphi_S = \frac{d_0}{2\pi}\frac{\cos\theta^*}{r^*} = \frac{d_0}{2\pi}\frac{x^*}{x^{*2}+K_F y^{*2}} \tag{20a}$$

$$\varphi_A = \frac{e_0}{2\pi}\frac{\sin\theta^*}{r^*} = \frac{e_0}{2\pi}\frac{y^*}{x^{*2}+K_F y^{*2}}\ , \tag{20b}$$

with d_0 and e_0 the adjustable strengths to be determined from matching. Furthermore, on using the Fourier integral, recognizing that

$$\frac{\partial\varphi_{SC}}{\partial Y}(X,\pm 1) = \frac{d_0}{(2\pi)\sqrt{K_F}}\frac{2X}{(1+X^2)^2}$$

$$\frac{\partial\varphi_{AC}}{\partial Y}(X,\pm 1) = \frac{e_0}{2\pi\sqrt{K_F}}\frac{1-X^2}{(1+X^2)^2}\ ,$$

the following representation of the complementary components φ_{SC} is obtained:

$$\varphi_{SC} = \frac{1}{\pi}\int_0^\infty dk \int_{-\infty}^{\infty} \cos k(X-\xi)\frac{\mathrm{ch}kY}{k\,\mathrm{sh}k}\left(\frac{d_0}{2\pi}\right)\frac{2\xi}{(1+\xi^2)^2}\,d\xi$$

$$= \frac{d_0}{2}\int_0^\infty \frac{\sin kX\,\mathrm{ch}kY}{\mathrm{sh}k}\,e^{-k}dk \simeq \frac{d_0}{2\pi K_F}\frac{\pi^2}{12}x^* + \ldots \text{ as } r^* \to 0\ . \tag{20c}$$

In a similar manner,

$$\varphi_{AC} = \frac{1}{\pi}\int_0^\infty dk \int_{-\infty}^{\infty} \cos k(X-\xi) \left\{\left(\frac{\sinh\gamma}{k\cosh k}\right)\frac{e_0}{2\pi\sqrt{K_F}}\frac{(1-\xi^2)}{(1+\xi^2)^2}\right\} d\xi$$

$$\simeq \frac{e_0}{2\pi\sqrt{K_F}}\frac{\pi^2}{24}\, y^* \text{ as } r^* \to 0 \quad , \tag{20d}$$

where the antisymmetric complementary component, φ_{AC} represents a divortex at the origin, which gives an induced upwash.

2.4 Matching

With the presumption that there is an overlap domain of validity of the inner (near field) representation of ϕ and its outer (far field) form, with no intermediate expansion required, appropriate developments in this domain for each are to be obtained in what follows. From these common representations, the unkown elements in both are determined by matching. Coordinates specifying the overlap domain are obtained from the ray preserving intermediate limit

$$x_\eta = \frac{x}{\eta(H)} \quad , \quad y_\eta = \frac{\tilde{y}}{\eta(H)} \text{ , fixed as } H \to \infty \quad ,$$

where $\eta(H) \to \infty$, is an order class intermediate between unity and H. Thus, $x^* = \frac{\eta}{H} x_\eta \to 0$, $y^* = \frac{\eta}{H} y_\eta \to 0$, and $x = \eta x_\eta \to \infty$. $\tilde{y} = \eta y_\eta \to \infty$. Also $r^* = \frac{\eta r_\eta}{H}$ with $r_\eta^2 = x_\eta^2 + K_F y_\eta^2$. The matching is effected by writing the inner and outer representations in terms of these intermediate variables. For the outer expansion, this is

$$\phi = \underset{①}{-\frac{\Gamma_F\theta}{2\pi}} + \frac{\pi^2}{24}\left(\frac{\Gamma_F}{2\pi}\right)\left(\frac{\eta}{H}\right)^2 \underset{⑥}{\frac{x_\eta}{\sqrt{K_F}}}\, y_\eta + \ldots + \frac{\ell n H}{H}\,\varphi_{\frac{1}{2}}\left(\frac{\eta}{H}, \frac{\eta}{H}, y_\eta\right)$$

$$+ \frac{1}{H}\frac{\gamma+1}{4K_F}\left(\frac{\Gamma_F}{2\pi}\right)^2\left\{\frac{\ell n \frac{\eta r_\eta}{H}}{\frac{\eta r_\eta}{H}}\cos\theta\right\} + \frac{1}{H}\frac{\gamma+1}{4K_F}\left(\frac{\Gamma_F}{2\pi}\right)^2\left\{\underset{③}{-\frac{1}{4}\frac{\cos 3\theta}{\frac{\eta r_\eta}{H}}}\right.$$

$$+ \underset{④}{\left(\ell n \frac{\pi}{4\sqrt{K_F}} + \frac{1}{4}\right)\frac{\cos\theta}{\frac{\eta r_\eta}{H}}} - \underset{⑦}{\frac{\pi^2}{24K_F}\frac{\eta x_\eta}{H}}\ell n \frac{\eta r_\eta}{H}$$

$$\left. - \underset{⑧}{\frac{\pi^2}{24}\ell n \frac{\pi^2}{4\sqrt{K_F}}\frac{\eta x_\eta}{HK_F}} - \underset{⑨}{\frac{\pi^2}{48}\frac{\eta \tilde{x}_\eta}{K_F H}}\cos 2\theta + \ldots\right\}$$

$$+ \underset{⑧}{\frac{1}{H}\frac{\gamma+1}{4K_F}\left(\frac{\Gamma_F}{2\pi}\right)^2\frac{\pi^2}{12}\frac{\eta x_\eta}{H}} + \ldots + \underset{④}{\frac{1}{H}\frac{d_0}{2\pi}\frac{\cos\theta}{\frac{\eta r_\eta}{H}}}$$

$$+ \underset{⑧}{\frac{1}{H}\frac{d_0}{2\pi K_F}\frac{\pi^2}{12}\frac{\eta x_\eta}{H}} + \underset{⑤}{\frac{1}{H}\frac{e_0}{2\pi}\frac{\sin\theta}{\frac{\eta r_\eta}{H}}} + \underset{⑩}{\frac{1}{H}\frac{e_0}{2\pi\sqrt{K_F}}\frac{\pi^2}{24}\frac{\eta y_\eta}{H}} + \ldots \quad , \qquad (21)$$

where similar terms have been identified with identical numerical labels for matching purposes. From the orders appearing in (21) a sharper lower bound for $\eta(H)$ is obtained giving

$$H^{2/3} << \eta << H \quad .$$

For the inner problem, if a new dependent variable is introduced, in which

$$\phi_1(x,\tilde{y}) \equiv \frac{K_C}{\gamma+1}\, x + \hat{\phi}_1 \ ,$$

then (6b) gives

$$(K-(\gamma+1)\phi_{0_x})\hat{\phi}_{1_{xx}} - (\gamma+1)\hat{\phi}_{1_x}\phi_{0_{xx}} + \phi_{1_{\tilde{y}\tilde{y}}} = 0 \ ,$$

and on the basis of the foregoing matching requires that

$$\hat{\phi}_1(x,\tilde{y}) = B_1 x\tilde{y} + P_1 x\ell nr + C_1\, x + Q_1 x\cos 2\theta + M_1\tilde{y} + N_1 - \frac{\Gamma_C\theta}{2\pi} + \ldots$$

or

$$\phi_1(x,\tilde{y}) = B_1 x\tilde{y} + P_1 x\ell nr + \left(\frac{K_C}{\gamma+1} + C_1\right)x + Q_1 x\cos 2\theta$$
$$+ M_1\tilde{y} + N_1 - \frac{\Gamma_C}{2\pi}\,\theta + \ldots \qquad (22)$$

in the far field $r = \sqrt{x^2+K_F y^2} \to \infty$, in which the constants B_1, P_1, C_1, M_1, N_1 and Q_1 are to be determined by the matching process. For this purpose, and inner solution is written in intermediate variables. The resulting expansion is

$$\phi = \underbrace{-\frac{\Gamma_F}{2\pi}\,\theta}_{①} + \underbrace{\left(\frac{\Gamma_F}{2\pi}\right)^2\frac{(\gamma+1)}{4K_F}\frac{\ell n\eta r_\eta}{\eta r_\eta}\cos\theta}_{②} \quad \underbrace{-\left(\frac{\Gamma_F}{2\pi}\right)^2\frac{(\gamma+1)}{16K_F}\frac{\cos 3\theta}{\eta r_\eta}}_{③} + \underbrace{\frac{D_0}{2\pi}\frac{\cos\theta}{\eta r_\eta}}_{④}$$

$$+\underset{⑤}{\frac{E_0}{2\pi}\frac{\sin\theta}{\eta r_\eta}}+O\left(\frac{\ell n^2\eta}{\eta^2}\right)+\frac{1}{H^2}\left\{\underset{⑥}{B_1\eta^2 x_\eta y_\eta}+\underset{⑦}{P_1\eta x_\eta \ell n\ \eta r_\eta}+\underset{⑧}{\left(\frac{K_C}{(\gamma+1)}+C_1\right)\eta x_\eta}\right.$$

$$\left.+\underset{⑨}{Q_1\eta x_\eta\cos 2\theta}+\underset{⑩}{M_1\eta y_\eta}-\frac{\Gamma_C}{2\pi}\theta+\ldots\right\}. \qquad (23)$$

In (23), the terms labeled ① , ② ,and ③ match automatically to their similarly labeled counterparts in (21) if the harmonic switchback term $\varphi_{\frac{1}{2}}$ is given by

$$\varphi_{\frac{1}{2}}=\frac{\gamma+1}{4K_F}\left(\frac{\Gamma_F}{2\pi}\right)^2\frac{\cos\theta}{r} \quad .$$

On the basis of comparison of the orders to be indicated, the following matchings apply:

$$O(\eta^{-1}):\ ④\Rightarrow\ \frac{D_0}{2\pi}=\left(\ell n\frac{\pi}{4\sqrt{K_F}}+\frac{1}{4}\right)+\frac{d_0}{2\pi}\ ,\ ⑤\Rightarrow\ \frac{E_0}{2\pi}=\frac{e_0}{2\pi} \qquad (24a)$$

$$O\left(\frac{\eta^2}{H^2}\right):\ ⑥\Rightarrow\ B_1=\frac{\pi^2}{24}\left(\frac{\Gamma_F}{2\pi}\right)\frac{1}{\sqrt{K_F}}\ ,\ ⑦\Rightarrow O\left(\frac{\eta}{H^2}\right):\ P_1=-\frac{\pi^2}{24K_F}\frac{\gamma+1}{4K_F}\left(\frac{\Gamma_F}{2\pi}\right)^2 \qquad (24b)$$

$$O\left(\frac{\eta}{H^2}\right):\ \textcircled{8} \Rightarrow \frac{K_C}{\gamma+1} + C_1 = -\frac{\gamma+1}{4K_F^2}\left(\frac{\Gamma_F}{2\pi}\right)^2\frac{\pi^2}{24}\,\ell n\frac{\pi}{4\sqrt{K_F}}$$

$$+\frac{\gamma+1}{4K_F}\left(\frac{\Gamma_F}{2\pi}\right)^2\frac{\pi^2}{12} + \frac{d_0}{2\pi K_F}\frac{\pi^2}{12} \qquad (24c)$$

$$\textcircled{9} \Rightarrow Q_1 = -\frac{\gamma+1}{4K_F^2}\left(\frac{\Gamma_F}{2\pi}\right)^2\frac{\pi^2}{48} \qquad (24d)$$

$$\textcircled{10} \Rightarrow M_1 = \frac{e_0}{2\pi\sqrt{K_F}}\frac{\pi^2}{24} \qquad (24e)$$

To complete the matching considerations, it is noted that a switchback term is required to match the term $\frac{\eta}{H^2}\frac{\gamma+1}{4K_F}\left(\frac{\Gamma_F}{2\pi}\right)\frac{\pi^2}{24K_F}\,x_\eta\,\ell nH$ arising from ⑦ in the outer expansion. Since this switchback term does not vanish at infinity, a corresponding switchback term can be added to the inner solution with a corresponding shift in the transonic similarity parameter. Accordingly, the revised inner expansions replacing (4a) and (5a) are

$$\phi = \phi_0 + \frac{\ell nH}{H^2}\,\phi_{\frac{1}{2}} + \frac{1}{H^2}\,\phi_1 + \ldots \qquad (4a')$$

$$K_T = K_F + \frac{\ell nH}{H^2}\,K_S + \frac{1}{H^2}\,K_C + \ldots \quad . \qquad (5a')$$

To match, therefore, $\phi_{\frac{1}{2}}$ is selected as

$$\phi_{\frac{1}{2}} = \frac{\gamma+1}{4K_F}\left(\frac{\Gamma_F}{2\pi}\right)^2\frac{\pi^2}{24K_F}\,x \quad , \qquad (25)$$

which satisfies the following switchback equation obtained by substitution of (4a') and (5a') into (3a):

$$(K_F-(\gamma+1)\phi_{0_x})\phi_{\ell_{xx}} - (\gamma+1)\phi_{\ell_{xx}}\phi_{0_{xx}} + \phi_{\ell_{yy}} = -K_S\phi_{0_{xx}} \quad , \quad O\left(\frac{\ell nH}{H^2}\right)$$

providing

$$K_S = \frac{(\gamma+1)^2}{4K_F^2}\left(\frac{\Gamma_F}{2\pi}\right)^2 \frac{\pi^2}{24} \quad . \tag{26}$$

This completes the matching. All the constants are given Eqs. (24), (25) and (26) with the exception of the doublet strengths D_0 and E_0. These are obtained from an extension of the integral equation analysis given in Ref. 12. Although the dominant term is given in Ref. 13, an analysis is required to obtain the doublet contributions which are higher order. The details are contained in the Appendix and the final results are

$$\frac{D_0}{2\pi} = \frac{A_w}{2\pi} + \frac{\gamma+1}{16K_F}\left(\frac{\Gamma_F}{2\pi}\right)^2 + \frac{\gamma+1}{2K_F}\left(\frac{1}{2\pi}\right)\int_0^1 \rho d\rho \int_0^{2\pi} \phi_{0_\xi}{}^2(\rho,\vartheta)d\vartheta$$

$$+ \frac{\gamma+1}{2K_F}\int_1^\infty \rho d\rho \int_0^{2\pi}\left(\phi_{0_\xi}{}^2 - \left(\frac{\Gamma_F}{2\pi}\right)^2 \frac{\sin^2\vartheta}{\rho^2}\right)d\vartheta \tag{27a}$$

$$\frac{E_0}{2\pi} = -\frac{\Gamma_F}{2\pi} + \frac{1}{2\pi}\int_{-1}^1 [\phi_0]d\xi \tag{27b}$$

$$A_w \equiv \int_{-1}^1 (F_u - F_\ell)d\xi$$

with ρ and ϑ as polar coordinates, and ξ is a dummy variable for x.

3.0 RESULTS

To obtain the wall interference corrections to be discussed in what follows, the free field problem (6a,c,e) was solved by the SLOR procedure of Ref. 12. The perturbation problem associated with (6b,d,e) with the far field (22) was solved with the linear counterpart of this method using modifications of special procedures to handle the perturbed shock waves developed by R.D. Small[14] to compute solutions of the lifting line problem formulated in Ref. 10.

As an indication of the size of the basic effect, surface pressures over a NACA 0012 airfoil at $M_F = 0.7$, $\alpha_F = 3.5°$, were computed for $A_c = K_c = 0$ for $H = 1$, or $h \approx 2$. The perturbation values are compared against those of the free field in Fig. 2 and show a surprisingly small interference effect for this small H value. For this and larger H, a part of this trend is associated with the small coefficients of the gauge functions of H appearing in (4a). A relevant factor may be the inability of the theory to generate a shock from an initially shockless flow. As in transonic lifting line theory, only shockless perturbations about shockless flows or shocked alterations about shocked cases are accessible to this theory. For the latter, the jump conditions given in Ref. 10 must be used for the linear variational problem ϕ_1, as previously indicated. When shocked perturbations occur on shockless flows, a special inner solution near the shock is required. In spite of these limitations, it is felt the theory of this report could provide useful information for the typical case in which shocked flows remained shocked.

In Fig. 3, free and confined chordwise pressures over the same NACA 0012 airfoil for different heights at a higher Mach number, $M_F = 0.75$ are shown. At the incidence indicated ($\alpha_F = 2°$), the typical supercritical pressure distributions are evident. As anticipated, the confined pressures approach the free field values as H increases.

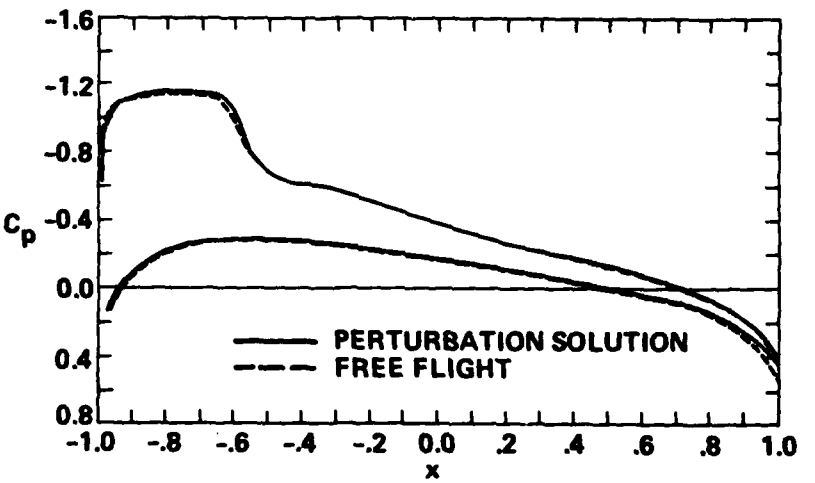

Fig. 2. Free and confined chordwise pressures NACA 0012 airfoil M_F=0.7, α_F=3.5°, A_C=K_C=0, H=1

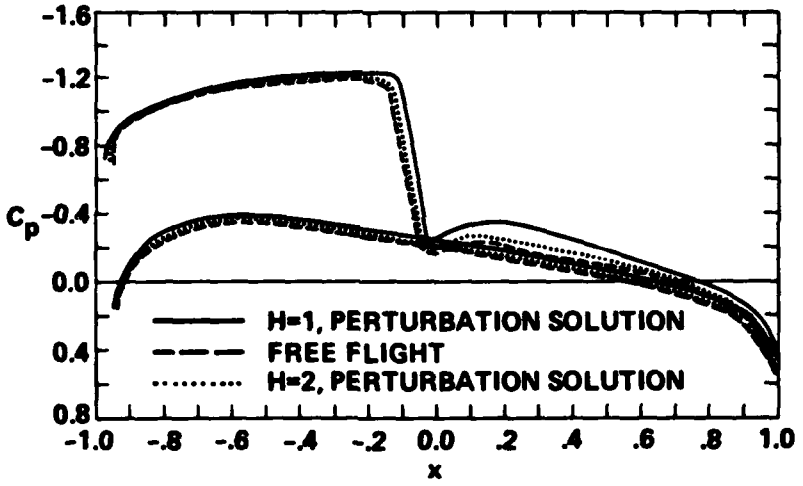

Fig. 3. Free and confined chordwise pressures NACA 0012 airfoil M_F=0.75, α_F=2°, A_c=K_c=0

A comparison of the perturbation solution of this report with that of the "exact" problem embodied in Eqs. (3) is shown in Fig. 4. The agreement is only fair for this low value of H with considerable degradation downstream of the shock. This may be related in some degree to the numerical approximations required to handle nodes in the vicinity of the shock, and the need for a local solution there.

As anticipated, the agreement between exact and perturbation solutions improves with an increase in H as shown in Fig. 5. However, here, there appears to be some deterioration near the trailing edge. In making these comparisons, a certain degree of sensitivity and nonuniqueness was experienced with respect to restarts of the exact and perturbation codes to obtain the various parametric ases. Multiple solutions and hysteretic behavior have been ascribed to underlying properties of the continuum problem in the free field case for the full potential equation in Ref. 15. The confined problem may also have these features. Since small differences are involved in the interference assessments, understanding the source of these nonuniquenesses deserves attention in future effort not only with asymptotic methods but in purely computational tunnel wall procedures as well. Other aspects associated with validations of this type relate to truncation errors of the computational solutions, the role of the far field, initial conditions for the SLOR algorithm and the degree to which the Kutta condition is satisfied.

As a further indication of the significance of some of these factors, the lift coefficients for the perturbation and exact solutions have been compared at various heights for the two cases considered in Figs. 1-4. In Table 1, excellent agreement is shown over the entire range of heights with some understandable increased discrepancy at H = 1. In view of the accuracy factors previously enumerated, this agreement is somewhat better than would be anticipated.

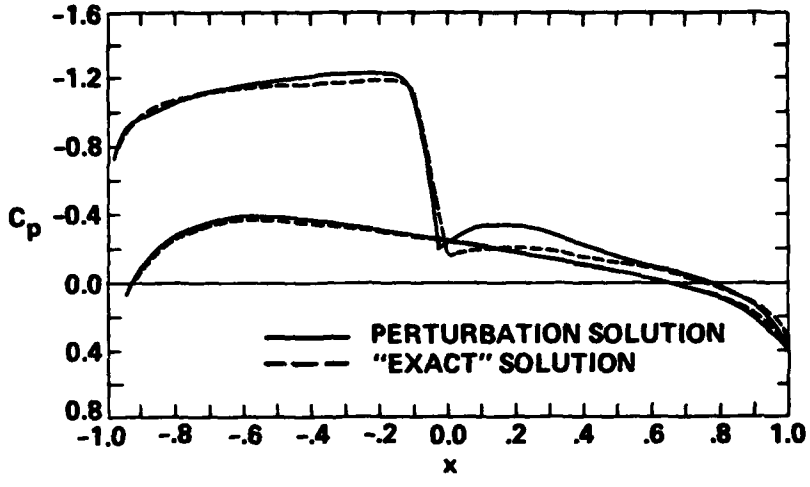

Fig. 4. Comparison between exact and approximate chordwise pressures on confined airfoil NACA 0012 airfoil M_F=0.75, α_F=2°, H=1, A_c=K_c=0

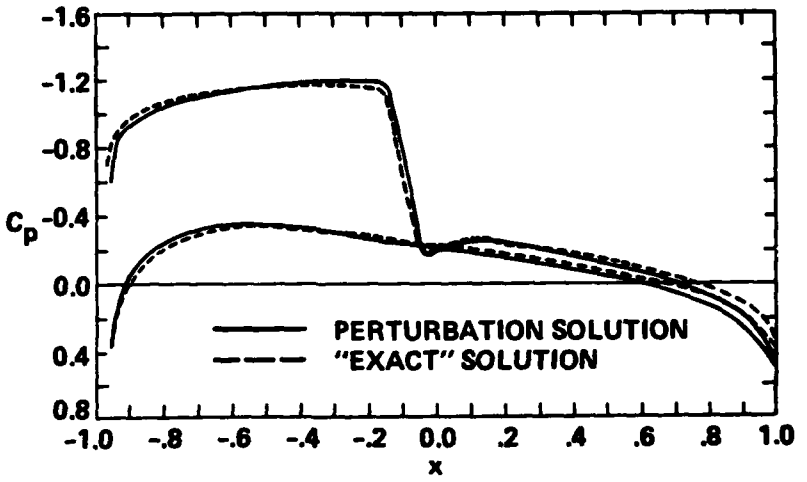

Fig. 5. Comparison between exact and approximate chordwise pressures on confined airfoil NACA 0012 airfoil M_F=0.75, α_F=2°, H=2, A_c=K_c=0

TABLE 1. COMPARISON OF LIFT COEFFICIENTS C_L FOR CONFINED NACA 0012 AIRFOIL AT VARIOUS WALL HEIGHTS, $M_F = .7$, $\alpha_F = 3.5°$

Method \ H	1	2	3	4	5
Exact	0.3655	0.3653	0.3652	0.3652	0.3652
Asymptotic Solution	0.3662	0.3654	0.3653	0.3652	0.3652

In Table 2, a similar comparison is shown, again indicating good agreement, but with increasing discrepancies at the lower H's.

TABLE 2. COMPARISON OF LIFT COEFFICIENTS C_L FOR CONFINED NACA 0012 AIRFOIL AT VARIOUS WALL HEIGHTS, $M_F = .75$, $\alpha_F = 2°$

Method \ H	1	2	3	4	5	6
Exact	0.4322	0.4256	0.4234	0.4234	0.4233	0.4234
Asymptotic Solution	0.4356	0.4264	0.4248	0.4242	0.4238	0.4237

It is interesting to note that strictly in accord with the asymptotic order of magnitude of the second order switchback term of Eq. (4a'), the perturbations associated with the solid walls are $O(\ell nH/H^2)$ which are smaller than the $O(H^{-1})$ one for the perturbation solution relevant to the porous case described in Ref. 8. Since porosity is introduced to weaken the wall interactions, this would superficially seem paradoxical. However, the coefficients of the indicated gauge functions of H do also play a role. From a numerical

viewpoint, these could effect the trend. Another perhaps more salient consideration deals with one motivation for porosity as a means of cancelling compression and expansion wave reflections. This mechanism is of limited relevance to the subsonic far field assumed in the formulation of this report. Accordingly, it is reasonable to state that whereas perforated walls can minimize supersonic wave reflection interference, they may not be optimum to reduce the subsonic constriction type. This aspect is probably related to the order of magnitude considerations mentioned previously.

Regarding interference minimization, Fig. 6 shows the interference lift C_{L_1} as a function of the tunnel wall interference angle of attack parameter A_C. The intersection with the absissca is the tunnel incidence correction required to produce the free field lift characteristics. Fig. 7 gives a similar curve at a larger Mach number but smaller geometric incidence requiring a larger A_C correction. In accord with (4a'), variations of this type can be used as a universal curve valid for arbitrary H's within assumptions of the asymptotic theory. A similar conclusion applies to the other forces and moments as well as the surface pressures. For pressures, the interference can only be reduced in a mean squared sense by adjusting A_C or K_C.

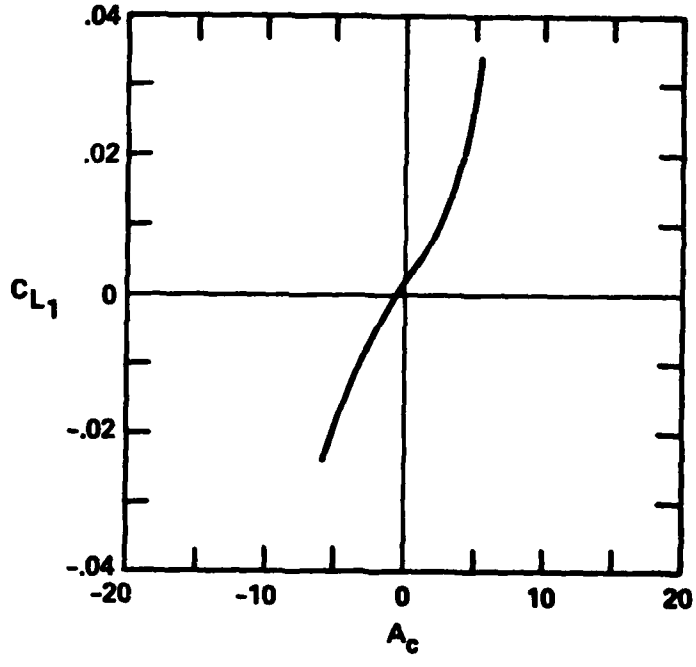

Fig. 6. Interference lift versus reduced angle of attack M_F=0.7, α_F=3.5°

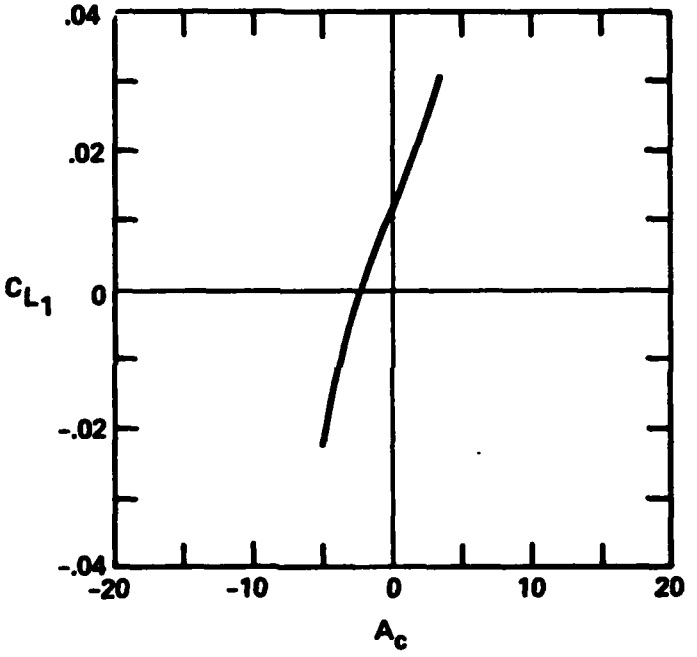

Fig. 7. Interference lift versus reduced angle of attack M_F=0.75, α_F=2°

4.0 CONCLUSIONS

An asymptotic theory of solid tunnel wall interference on transonic airfoils has been developed based on the limit of large wall height within the Karman Guderley (KG) theory. This approximation leads to a singular perturbation problem in which the near field approximation of weak linear perturbations about the KG small disturbance model is non-uniformly valid as the walls are approached. A far field for the near field problem comes from an "outer" approximation involving wall reflections of a multipole representation of the airfoil dominated by a reflected potential vortex. From the analysis and results, the following observations can be made:

- Switchback terms are needed in the transonic case to properly match the near and far fields. These alter the effective similarity parameter of the confined flow field.

- Perturbations of the pressures and forces in the near field are $O(\ell nH/H^2)$.

- The asymptotic theory provides good agreement with the exact KG model for large to moderate H.

- The usefulness of the theory is enhanced by the fact that it separates H out of the interference problem and requires the solution of a nonlinear and linear problem rather than two nonlinear problems representing respectively the free and confined fields to obtain the interference correction.

The procedures developed in this report provide a basis for extension to three-dimensional and unsteady problems. Lifting line and slender body theory can supply the necessary starting points for the former.

5.0 REFERENCES

1. Garner, M.C., Rogers, E.W.E., Accum, W.T.E.A., and Maskell, E.E., "Subsonic Wind Tunnel Wall Corrections," AGARDograph 109, October 1966.

2. Pindzola, M., and Lo, C.F., "Boundary Interference at Subsonic Speeds in Tunnels with Ventilated Walls," AEDC-TR-69-47 (AD 687440), May 1969.

3. Mokry, M., et al, "Wall Interference on Two-Dimensional Supercritical Airfoils Using Pressure Measurements to Determine the Porosity Factors for Tunnel and Ceiling," NRC (Canada) LR-575, February 1974.

4. Kraft, E.M., and Dahm, W.J.A., "Direct Assessment of Wall Interference in a Two-Dimensional Subsonic Wind Tunnel," AIAA Paper 82-0187, presented at the 20th Aerospace Sciences Meeting, Orlando, Florida, January 11-13, 1982.

5. Murman, E.M. "A Correction Method for Transonic Wind Tunnel Wall Interference," AIAA Paper No. 79-1533, 1979.

6. Kemp, W.R., Jr., "Toward the Correctable - Interference Transonic Wind Tunnel," AIAA 9th Aerodynamic Testing Conference, 1976, pp. 31-38.

7. Rizk, M.H., Hafez, M., Murman, E.M., and Lovell, D., "Transonic Wind Tunnel Wall Corrections for Tpree-Dimensional Models," AIAA Paper 82-0588, AIAA 12th Aerodynamic Testing Conference Proceedings, March 22-24, 1982, pp. 120-130.

8. Chan, Y.T., "A Singular Perturbation Analysis of Two-Dimensional Wind Tunnel Interferences," ZAMP, 31, 1980, pp. 605-619.

9. Van Dyke, M., Perturbation Methods in Fluid Mechanics, the Parabolic Press, Stanford, Calif., 1975.

10. Cook, L.P., and Cole, J.D., "Lifting Line Theory for Transonic Flow, SIAM J Appl. Math., 35, 2, September, 1978, pp. 209-228.

11. Van Dyke, M.D., "A Study of Second Order Supersonic Flow Theory," NACA Report 1081, 1952.

12. Murman, E.M., and Cole, J.D., "Calculations of Plane Steady Transonic Flow," AIAA J. 9, 1, January 1971, pp. 114-121.

13. Klunker, E.B., and Newman, P.A., "Contributions to Methods for Calculating the Flow About Thin Lifting Wings at Transonic Speeds - Analytical Expression for the Far Field," NASA Report TN D-6530, 1971.

14. Small, R., "Calculation of Transonic Lifting Line Theory," Israel J. of Tech., 19, 1981, pp. 26-33.

15. Steinhoff, J., and Jameson, A., "Multiple Solutions of the Transonic Potential Flow Equation," AIAA Paper No. 81-1019 in Proceedings of AIAA 5th Computational Fluid Dynamics Conference, Palo Alto, Calif., June 22-23, 1981.

APPENDIX

Determination of E_0 and D_0

Using Green's theorem in a manner similar to that given in Ref.12, the integral equation obtained for ϕ_0 is

$$\phi(X,Y) = \int_{-1}^{1} S_w [\phi_\eta]_w d\eta - \int_{-1}^{1} \left[\frac{\partial S}{\partial \eta}\right]_w [\phi]_w \, d\xi - \Gamma \int_{1}^{\infty} \left(\frac{\partial S}{\partial \eta}\right)_w d\xi - \frac{\gamma+1}{2K} I \,, \qquad (A1)$$

where the subscripts on ϕ have been dropped, $[f]_w = f_{y=0+} - f_{y=0-}$, with a change of notation from the previous sections, $X = x$, $Y = \sqrt{K_F}\,\tilde{y}$, $S = \frac{1}{2\pi} \ell n \sqrt{(x-\xi)^2+(Y-\eta)^2}$, $\Gamma = [\phi]_{w_{x=1}}$, ξ and η are dummy versions of X and Y and

$$I \equiv \iint_{-\infty}^{\infty} S_\xi(X,Y,\xi,\eta)\phi_\xi^2(\xi,\eta)\, d\xi d\eta \quad . \qquad (A2)$$

Ref. 12 is restricted to the nonlifting case, and in that situation, ϕ_ξ^2 dies off sufficiently rapidly so that a convergent integral involving the average source strength is obtained by placing the S_ξ kernel in (A2) outside the integral signs. This is true since ϕ in the nonlifting case is asymptotically a doublet and is $O(r^{-1})$ as $r \to \infty$. By contrast, ϕ is a potential vortex in accord with (7a) and ϕ_ξ can no longer be regarded as approximately of compact support. To deal with this difficulty, I is written in the following form:

$$I = I_1 + I_2 + I_3 \quad . \qquad (A3)$$

where

$$I_1 = \int_0^1 d\rho \int_0^{2\pi} S_\xi \phi_\xi^2 \, \rho \, d\vartheta \tag{A4}$$

$$I_2 = \int_1^\infty \rho d\rho \int_0^{2\pi} S_\xi \left(\phi_\xi^2 - \left(\frac{\Gamma}{2\pi} \right)^2 \frac{\sin^2 \vartheta}{\rho^2} \right) d\vartheta \tag{A5}$$

$$I_3 = \int_1^\infty \rho d\rho \int_0^{2\pi} S_\xi \left(\frac{\Gamma}{2\pi} \right)^2 \frac{\sin^2 \vartheta}{\rho^2} \, d\vartheta$$

$$S_\xi = -\left(\frac{1}{2\pi} \right) \frac{(R\cos\theta - \rho\cos\vartheta)}{R^2 - 2R\rho\cos(\theta - \vartheta) + \rho^2}$$

$$X = R\cos\theta, \; \xi = \rho\cos\vartheta \; .$$

In (A3), I has been regularized at ∞ by subtracting and adding the asymptotic representation of ϕ_ξ^2 in that neighborhood. A resulting singularity near the origin is avoided by decomposing the integral into a part inside the unit circle and outside of it. Since its integrand is of compact support, I_1 can be approximated by the method of Ref. 12, i.e., approximation of the integrand for large R and integration term by term. The same conclusion applies to I_2, whose integrand is $O\left(\frac{\ell n R}{R^3}\right)$ as $R \to \infty$. The integral I_3 can be treated exactly. However, the operations have to be performed with great care because of the discontinuous nature of the integrand. The choice of the lower ρ limit as unity in (A4) and (A5) leads to considerable simplifications as compared to other values and therefore was adopted.

The results for I_1, I_2, and I_3 are

$$I_1 \simeq -\left(\frac{1}{2\pi} \right) \frac{\cos\theta}{R} \int_0^1 \rho d\rho \int_0^{2\pi} \phi_\xi^2 \, d\vartheta \tag{A6}$$

$$I_2 \simeq \left(\frac{1}{2\pi}\right)\frac{\cos\theta}{R}\int_1^\infty \rho d\rho \int_0^{2\pi}\left(\phi_\xi^2 - \left(\frac{\Gamma}{2\pi}\right)^2 \frac{\sin^2\vartheta}{\rho^2}\right) d\vartheta \qquad (A7)$$

$$I_3 \simeq -\left(\frac{\Gamma}{2\pi}\right)^2 \frac{\ell nR}{2R}\cos\theta - \left(\frac{\Gamma}{2\pi}\right)^2 \frac{\cos\theta}{8R} + \left(\frac{\Gamma}{2\pi}\right)^2 \frac{\cos 3\theta}{8R} \qquad (A8)$$

which upon substitution in (A1) and approximation of the one-dimensional integrals therein leads to (27).